



Review—Cobalt Thin Films: Trends in Processing Technologies and Emerging Applications

Alain E. Kaloyeros,¹ Youlin Pan,² Jonathan Goff,² and Barry Arkles^{1,2,z}

¹SUNY Polytechnic Institute, Albany, New York 12203, USA

²Gelest, Inc., Morrisville, Pennsylvania 19067, USA

Cobalt metallic films are the subject of an ever-expanding academic and industrial interest for incorporation into a multitude of new technological applications. This report reviews the state-of-the-art chemistry and deposition techniques for cobalt thin films, highlighting innovations in cobalt metal-organic chemical vapor deposition (MOCVD), plasma and thermal atomic layer deposition (ALD), as well as pulsed MOCVD technologies, and focusing on cobalt source precursors, thin and ultrathin film growth processes, and the resulting effects on film composition, resistivity and other pertinent properties.

© The Author(s) 2019. Published by ECS. This is an open access article distributed under the terms of the Creative Commons Attribution 4.0 License (CC BY, <http://creativecommons.org/licenses/by/4.0/>), which permits unrestricted reuse of the work in any medium, provided the original work is properly cited. [DOI: [10.1149/2.0051902jss](https://doi.org/10.1149/2.0051902jss)]



Manuscript submitted January 2, 2019; revised manuscript received February 4, 2019. Published February 27, 2019.

An increasing level of research and development (R&D) activity is now focused on cobalt thin and ultrathin film structures, which have found myriad new applications across a variety of industrial sectors.^{1,2} This attraction to cobalt is driven by its appealing physical, mechanical and electrical properties.^{3,4} In particular, metallic cobalt films play a key role in the reliability of integrated circuitry (IC) devices, as metallic cobalt films' greater resistance to electromigration and lower tendency to undergo diffusion gives them a higher comparative stability relative to copper (Cu) in environments that involve both elevated temperature and high current density induced stresses.

These salient properties have compelled consideration for a wealth of applications in IC systems, both in traditional architectures as well as novel systems associated with cobalt magnetic dipole moment, such as spintronic and giant magnetoresistance (GMR) devices.^{5–10} IC device manufacturers recently reporting the use of cobalt in nanoscale metallization architectures include Intel, TSMC and Samsung—having introduced it at the 10, 14 and 16nm nodes, respectively.^{11,12} In addition, cobalt's use as an actual conductor in nanoscale topographies is currently believed to be in limited production.

Further advantage for IC technologies includes the fact that cobalt (Co) thin films can act as seed layers for electroplated cobalt and undergo post-deposition conversion to binary element compounds such as cobalt silicide, cobalt sulfide, cobalt oxide and metallic alloys. For example, cobalt silicide (CoSi₂) conversion coatings¹³ are emerging as a viable replacement for titanium silicide in self-aligned silicide (salicide) applications due to wider silicidation window, which is consistent with the requirements for generating finer line geometries.

These commercial usages have spawned tremendous interest not only in optimizing and understanding Co film growth processes and resulting properties, but also in expanding their use in future IC products. Other uses of metallic cobalt and cobalt containing films (such as oxides, sulfides, silicides and nitrides) include magneto-optic recording media,¹⁴ data storage,^{15,16} sensor technologies,^{15,17–19} catalysts for growing carbon nanotubes and self-aligned nanowires,^{15,18,19} reflective thin films for optical devices¹⁷ and, more broadly, as antibacterial,^{18,19} decorative, protective¹⁷ and wear-resistant coatings.²⁰

Given cobalt's increasing potential to continue enabling exciting innovations across numerous industrial sectors, this article presents an overview of recent advancements in Co vapor phase processing techniques and their impact on film physical, chemical and electrical properties. While there is a broad literature on liquid phase deposition (electroplating) for cobalt, cobalt oxide and cobalt sulfide, this focuses predominantly on industrial finishes, with a smaller representation in photovoltaic & storage devices.^{21–23} Only a very limited number of recent reports have been published on electroplating

of Co for IC applications.^{24,25} Similarly, a large literature describes the use of non-metallic cobalt films in the hydrothermal conversion of cobalt salts. Although examples of these methods are included in this review when scientifically and technologically relevant,²⁶ the vast majority of recent R&D efforts have centered on the growth of Co thin films through vapor phase deposition techniques. Accordingly, this article will primarily summarize and discuss the most recent work in such techniques—namely: thermal metal-organic chemical vapor deposition (MOCVD) and pulsed thermal MOCVD, as well as thermal, plasma and area-selective atomic layer deposition (ALD).

It is worth noting that the literature provides a complex representation of the thermal, chemical, electrical, compositional and morphological characteristics of Co thin films. This complexity is due to the fact that, in many cases, film properties are reported for the specific deposition process used to grow the Co thin films, while associated film morphologies, compositions and impurity levels are often neither comprehensively defined nor thoroughly reported. This review therefore focuses on specific film properties and performance as they relate to specific Co processing technologies, with a particular emphasis on IC metallization. Given the rapid evolution of cobalt deposition technologies, the majority of reports summarized and discussed here were published within the last ten years; however, earlier work is referenced and reviewed as needed in order to place more recent work in the appropriate context.

Fundamental Properties of Cobalt

Any review of the latest accomplishments in Co processing technologies must begin with a summary of metallic cobalt's fundamental properties. There are two primary Co crystalline configurations of metallic cobalt: face-centered-cubic (fcc) and hexagonal close packed (hcp).^{27,28} However, there is currently no data compilation that comprehensively describes the properties of Co thin films. Co thin film data in the literature is often incompletely characterized in terms of crystallinity, domain size and other morphological characteristics; this is also true in regards to compositional aspects, since the incorporation into Co thin films of low atomic percentages of other elements—such as C, O and H (as a result of the deposition process), as well as other elements such as Si and Cu (as a result of inter-diffusion with the substrate during deposition)—is not always considered or fully reported.

Table I displays nominal properties for cobalt and selected cobalt binary compounds associated with semiconductor applications. The data presented should be viewed by the reader as guide, but should not be taken as specific to any particular Co thin film formed by any of the techniques discussed herein. The information is meant to represent relevant, albeit not absolute, properties of Co films obtained at temperatures in the range of 20°–100°C, with the obvious

^zE-mail: executiveoffice@gelest.com

Table I. Overview of Pertinent Properties of Cobalt.

	Elemental Cobalt					
	Bulk	Thin Film		Binary Cobalt Systems		
		MOCVD	ALD	Cobalt Disilicide	Cobalt Sulfide	Cobalt Oxide
Formula	Co	Co	CoSi ₂	CoS	CoO	
Atomic/Molecular Weight	58.933	58.933	115.10	91.00	74.93	
Thermal						
Transformation temp, °C (hcp to fcc)	417°					
H transformation J/g	251					
Melt Point	1493°			1277°	1182°	1800°
heat of fusion J/g	259.4					
Boiling Point, °C	3100°					
heat of vaporization J/g	6276					
Specific heat J/g.°C	0.442					
Coefficient of Thermal Expansion, x 10 ⁻⁶ , °C ⁻¹				~10		
hcp, 25°C	12.5					
fcc, 417°C	14.2					
Thermal conductivity (25°C), W/m·K	69.2					
Curie Temp, °C	1121°					
Electrical						
Resistivity (20°C), μ ·cm	6.2	8.5 ³ 17* ¹²	23* ²³	10-25	2000-3500	1.1 × 10 ⁵
Dielectric Constant					3.241	12.9*
Electrochemical Potential (EMF-aqueous),V	0.277 (+2)					
Magnetic						
Permeability μ: initial; max	68; 245					
Residual induction, T°	0.490					
Coercive force, A/m	708					
Mechanical						
Youngs Modulus (20°C), GPa	211					
Tensile Strength (annealed), MPa	588					
Shear modulus, GPa	82.6					
Poisson's Ratio	0.32					
Hardness, Vickers MPa	1043					
Density, g/cm ³	8.90			5.3	5.45	6.41
Optical						
Refractive index, 589nm	2.142			3.094	~2.5	2.33
Band gap, eV					1.35-1.6	2.4
Other						
Diffusion Rate in Si, cm ² /s	10 ⁻⁶ – 10 ⁻⁴					
Activation Energy (eV) (for diffusion in Si)	2.8					

The data reported here is compiled from various sources^{68,70-74} and should be viewed as guideline data for Co properties rather than absolute values.

*Film resistivity/dielectric properties highly dependent on film thickness and purity level.

exception of thermal properties, and offers the reader a foundation for the study and examination of Co film properties as reported in the literature.

Overview of Cobalt Thin Film Vapor Phase Deposition Techniques

A cursory reading of the literature in this area quickly reveals both inconsistencies in precursor naming and a lack of universally accepted chemical acronyms. For the most part, the compound name in the primary reference has been retained in this review. However, in order to provide consistency for the reader, we have assigned an identification number to any precursor mentioned more than once for which a discrete chemical structure has been reported, as outlined in Table II. Within the text of this review, the identification numbers listed in Table II appear next to the precursor name used, and track to Chemical Abstract Systems (CAS) registration numbers. Table III presents a summary of recent MOCVD and ALD Co modeling

and mechanistic studies,⁵⁻⁷ while Table IV contains a synopsis of recent thermal MOCVD Co reports;^{8-10,14-19,29-34} Table V provides summaries of recent pulsed thermal MOCVD and plasma and thermal ALD studies,^{20,26,35-54} and Table VI gives an outline of recent area-selective ALD work.^{26,51,55-66}

As in many material systems, the evolution in Co processing protocols has proceeded from MOCVD-based to ALD-based technologies, a trend driven by the need for highly conformal ultra-thin Co films with well-defined composition and characteristics to be included in the reduced geometries and features of future devices, led by the IC and solar cell industries.

Thermal Co MOCVD is characterized by substrate surface driven reactions capable of yielding improved step coverage in aggressive device structures. Reactants, including a Co source precursor, are usually transported simultaneously in the gas phase to the substrate surface.⁸⁻¹⁰ The reactants then adsorb onto the substrate surface, with subsequent surface diffusion and desorption of some reactants or reactant species. Surface reactions follow, with film nucleation and

Table II. Cobalt Precursor Identification Numbers and CAS registration.

Oxidation State	Name	Formula/Abbreviated Structure	Identification	CAS #
Co ⁽⁰⁾	Dicobalt octacarbonyl	Co ₂ (CO) ₈	Co-001	10210-68-1
	Cobalt tricarbonyl nitrosyl	Co(CO) ₃ NO	Co-002	14096-82-3
	Dicobalt hexacarbonyl t-butylacetylene (CCTBA)	Co ₂ (CO) ₆ (η ² -HC≡Ct-Bu)	Co-003	56792-69-9
	Dicobalt hexacarbonyl trimethylsilylacetylene	Co ₂ (CO) ₆ (η ² -HC≡CSiMe ₃)	Co-004	57032-12-9
	Dicobalt hexacarbonyl bis(trimethylsilyl)acetylene	Co ₂ (CO) ₆ (η ² Me ₃ SiC≡CSiMe ₃)	Co-005	14767-82-9
Co ^(I)	Hydridocobalt carbonyl	HCo(CO) ₄	Co-101	16842-03-8
	Trifluoromethyl cobalt carbonyl	CF ₃ Co(CO) ₄	Co-102	15892-59-8
	η ⁵ -Cyclopentadienylcobalt carbonyl	CpCo(CO) ₂	Co-103	12078-25-0
	η ⁵ -Pentamethylcyclopentadienylcobalt dicarbonyl	Cp*Co(CO) ₂	Co-104	12129-77-0
	η ⁵ -Cyclopentadienylcobalt bis(ethylene)	CpCo(CH ₂ = CH ₂) ₂	Co-105	69393-67-5
	η ⁵ -Cyclopentadienylcobalt bis(trimethylsilyl)ethylene	CpCo[Me ₃ SiCH = CH ₂] ₂	Co-106	189282-65-3
	η ⁵ -Cyclopentadienylcobalt 1,5-cyclooctadiene	Cp(Co(COD))	Co-107	12184-35-9
	(η ³ -t-Butylallyl)cobalt tricarbonyl	(t-Bu-allyl)Co(CO) ₃	Co-108	1263431-26-0
	Cobalt dicarbonyl[1,3-dihydro-1,3-bis(1-methylene)-2H-imidazol-2-ylidene] nitrosyl	Co(Dipp ₂ Im) (CO) ₂ (NO)	Co-109	1869928-52-8
	Cobalt trimethylphosphine dicarbonyl[1,3-dihydro-1,3-bis(1-methylene)-2H-imidazol-2-ylidene]nitrosyl	Co(Dipp ₂ Im) (CO) ₂ (PMe ₃)(NO)	Co-110	2205068-13-7
	Co ^(II)	Cobalt bis(acetylacetonate)	Co(acac) ₂	Co-201
Cobalt bis(2,2,6,6-tetramethylheptan-3,5-dionate)		Co(tmhd) ₂	Co-202	13986-53-3
Cobaltocene		CoCp ₂	Co-203	1277-43-6
Bis(methylcyclopentadienyl)cobalt		Co(MeCp) ₂	Co-204	12146-91-7
Bis(η ⁵ -pentamethylcyclopentadiene)cobalt		(Cp*) ₂ Co	Co-205	74507-62-3
Bis(N,N'-diisopropylacetamidinato)cobalt		Co(i-Pr-AMD) ₂	Co-206	635680-58-9
(N,N'-diisopropylacetamidinato)(η ⁵ -pentamethylcyclopentadiene) cobalt		Cp*Co(i-Pr-AMD)	Co-207	1206524-90-4
Bis(1,4-di-t-butyl-1,3-diazabutadienyl)cobalt		Co(^t -Bu ₂ DAD) ₂	Co-208	177099-51-3
N-t-butyl-N-ethylpropinamidinato)cobalt		Co(AMD) ₂	Co-209	1014477-51-2
Co ^(III)		Cobalt tris(tetramethylheptanedionate)	Co(tmhd) ₃	Co-301
	η ⁵ -Cyclopentadienyl-N,N'-diisopropyl-1,4-diazabutadienyl cobalt	CpCo(i-Pr ₂ dab)	Co-302	101178-17-0
	η ⁵ -Cyclopentadienyl-N,N'-di-t-butyl-1,4-diazabutadienyl cobalt	CpCo(t-Bu ₂ dab)	Co-303	101178-18-1

Table III. Summary of Recent ALD and MOCVD Cobalt Modeling and Mechanistic Studies.

Modeling Technique	Precursor class	Brief Description	Reference
Experimental surface-science studies of surface reaction mechanisms associated with ALD processes.	Various inorganic and organic precursors including: (a) TiCl_4 ; (b) Cu metallorganic compounds such as $\text{Cu}^{\text{I}}\text{-N,N'-di-}is-butylacetamidate and \text{Cu}^{\text{II}}(\text{acac})_2 (Co-201); (c) tetrakis(dimethylamido)Ti (TDMAT) and tetrakis(ethylmethylamido)Ti (TEMAT), as well as pentakis(dimethylamido)Ta (PDMAT); (d) \text{Sr}_2(2\text{-}it-butyl-4,5-t-amylimidazolyl)_4 (\text{Sr}_2(\text{Ztpp})_4); (e) \text{Fe}(\text{CO})_5; and (f) \text{MeCpMn}(\text{CO})_3.$	Despite no reporting of ALD Co work, a good review of ALD fundamentals that provides a solid foundation for understanding key ALD growth mechanisms. Focused primarily on the role of the substrate surface and co-reactants in catalyzing and enabling the ALD reaction. In particular, this study compares ALD nucleation and growth on semiconducting and insulating surfaces versus conducting (metallic) surfaces for a variety of inorganic and metal-organic precursors.	⁵ Zaera et al. (2013)
Summary of experimental studies of the reaction pathways that underline the effects of co-reactants in ALD and pulsed MOCVD.	3 Co precursors and reaction chemistries discussed: (a) $\text{Co}_2(\text{amdiPr})_2$ (Co-206) with H_2 ; (b) $\text{Co}_2(\text{amdiPr})_2$ (Co-206) with NH_3 ; and (c) [(<i>t</i> -Buallyl)Co(CO) $_3$] (Co-108) in combination with dimethylhydrazine $\text{N}_2\text{H}_2\text{Me}_2$.	A review of the role of three reaction chemistries in ALD Co on various surfaces. Presents a comparative analysis of reactions that yield Co metal directly versus reactions that form intermediates in the substrate surface which subsequently decompose to Co metal.	⁶ Emslie et al (2013) ⁶⁰ Kwon et al 2012
Theoretical study of thermal ALD using density functional theory calculations.	Co from Co(<i>t</i> -butylallyl) (CO) $_3$ (Co-108) and dimethylhydrazine (H_2NNMe_2) in the study of redox adsorption of Co source precursors. Co from complexes with “non-innocent” ligands for Co ALD from zero-valent Co precursors such as diazadienyl molecules <i>t</i> Bu $_2$ DAD (Co-208) and Me_2DAD ($\text{C}_4\text{H}_8\text{N}_2$).	Study of the underlying mechanisms for ALD Co based on mechanistic information from density functional theory calculations for abbreviated cycles in H_2 -based reactions. This study examines how ligands may be cleanly eliminated and explores the possibility of certain side-reactions that yield impurities such as C, as well as potentially other undesired products such as CoO.	⁷ Elliott et al. (2017)

Table IV. Summary of Recent Thermal MOCVD Cobalt Work.

Deposition Technique	Potential Applications	Brief Description	Reference
Thermal MOCVD	Cobalt silicides for Ohmic contacts in IC applications	Co and CoSi ₂ thin films	³ Ivanova et al. (1999)
Thermal MOCVD	High catalytic activity, antiferromagnetism, electrochromism, magnetic detectors, membranes for oxidation of hydrocarbons, counter electrodes, humidity or oxygen optical sensors, solar-selective absorbers and protective layers	Co ₃ O ₄ thin films	⁶⁷ Pasko et al. (2004)
Pulsed Spray Evaporation MOCVD (PSE-MOCVD) system	Thin films for electrical, magnetic, and catalytic applications	Co and Co alloys (CoC ₂ and CoO _x) thin films	⁸ Premkumar et al. (2007)
No actual deposition. Only structural and chemical characterization of Co precursors	Magnetic multilayered structures, spin valves and granular alloys for potential giant magnetoresistance (GMR) devices	Co(acac) ₂ (Co-201). Inclusion complex of β-cyclodextrin with cobalt iodide (CoI ₂)	⁹ Papadopoulos et al. (2008)
Thermal MOCVD	Co silicide as contact material in MOS field effect transistor (MOSFET)	CoSi thin films	¹⁰ Lee et al. (2008)
Thermal MOCVD in a cold wall reactor	Co thin films and nanostructures as active materials in IC, sensors and catalysts. Reflective and refractive coatings for optical devices. Decorative and/or protective coatings	Co and CoO _x nanoparticles	¹⁷ Pugh et al. (2013)
Thermal MOCVD in a cold wall reactor	As diffusion barrier for Cu in multilevel metallization in IC applications	ALD CoW thin films	³⁴ Shimizu et al. (2013)
Thermal MOCVD in home-made vertical cold wall reactor	Sensors, magnetic information storage material, antibacterial coating, seed material for the growth of carbon nanotubes, and giant magnetoresistance (GMR) effect in multilayered structures	Films consisting of mixture of Co and CoO _x Metallic Co thin films	¹⁸ Georgi et al. (2013) ²⁹ Georgi et al. (2014)
Thermal MOCVD	Cu Metallization in integrated circuitry (IC)	Co(W) adhesion layers for Cu metallization for integrated circuitry interconnects applications	³⁰ Shima et al. (2014)
Thermal MOCVD	Magneto-optic recording media and spintronic devices	Metallic Co thin films	¹⁴ Dorovskikh et al. (2016)
Cyclic Thermal MOCVD system	Data storage devices and sensors. Cobalt silicides for Ohmic contacts in IC applications and as catalyst to grow aligned nanowires	Metallic Co thin films	¹³ Samal et al. (2014)
Thermal MOCVD	Optical sensors, magnetic detectors, catalytic membranes, solar selective absorbers, anode material for lithium ion batteries	Metallic Co, Co(II) oxide (CoO) or Co(II,III) oxide (Co ₃ O ₄)	⁷⁵ Schmid et al. (2014)
Pulsed Spray Evaporation MOCVD (PSE-MOCVD) system	N/A	CoO _x thin films	³¹ Weiss et al. (2015)
Direct-liquid-evaporation MOCVD (DLE-MOCVD) system	Giant magnetoresistance (GMR) devices, spintronics, Co or Co-based alloy as effective adhesion layers in Cu interconnects, wetting layer to induce void-free filling of narrow copper lines by reflow of nonconformal PVD Cu, IC device contacts	Metallic Co thin films	³² Yang et al. (2015)
Thermal MOCVD	Magnetic information storage and sensor systems, especially given giant magneto resistance (GMR) effect in multilayered stacks with Co and non-ferromagnetic films, antibacterial coatings, catalyst nanoparticles for the growth of carbon nanotubes	Films consisted of 45.3% Co, 38.1% O, 11.7% P and 4.9% C, indicating the presence of metallic Co, Co phosphate, Co oxide and Co carbide	¹⁹ Georgi et al. (2015)
Thermal MOCVD in an atmospheric pressure reactor	Replacement for Ta as seed layer and liner in IC Cu metallization. Co ferromagnetic films layered with nonmagnetic metals for GMR devices for use in magnetic data storage media. Effective catalyst in Fischer-Tropsch (FT) process	Metallic Co thin films	¹⁶ Hamilton et al. (2016)
Thermal MOCVD in hot wall reactor	N/A	Stoichiometric Co ₃ O ₄ thin films	³³ Zhang (2018)

Table V. Summary of Recent Pulsed MOCVD and ALD Cobalt Work.

Deposition Technique	Potential Applications	Brief Description	Reference
Thermal ALD	Electrochromic devices and windows, non-emitting displays, smart windows, thermal control for space vehicles, selective absorbers and corrosion protective coatings in solar cells, magnetostrictive torque sensors, magnetic recording media, spin valve pinning layers, rechargeable batteries, oxidation catalysts, gas sensors, and cathodes in high temperature ceramic fuel cells	Growth of polycrystalline Co ₃ O ₄ from Co(thd) ₂ (Co-202) in the temperature range of 114–307°C. Preferred (100) orientation observed on all substrate types at lower substrate temperatures. Preferred (111) orientation seen on Si(111) at higher substrate temperatures, while films on soda lime glass were unoriented.	⁴⁵ Klepper et al. (2007)
Thermal ALD	Catalysis, electrochromic materials (e.g., in smart windows), applications that exploit magnetic properties, solid oxide fuel cells	Growth of polycrystalline Co ₃ O ₄ from CoCp ₂ (Co-203) in the temperature range of 137–285°C. Formation of CoO as secondary phase at 331°C	⁴⁸ Diskus et al. (2011)
Plasma-enhanced ALD (PE-ALD)	Contact material for nanoscale electronic devices	Systematic study of the role of N in the PE-ALD process by varying the N ₂ /H ₂ gas flow ratio	⁵¹ Yoon et al. (2011)
Thermal ALD	Conformal coating of porous oxide structures without blocking the nanoporosity for ferromagnetic, high refractive index, and mechanical strength applications	Growth of CoO coatings on γ -alumina nanoporous particles with sizes ranging from 20 to 100 μ m in diameter, and Al membrane discs (anodiscs) to convert their surfaces into nanoporous, mechanically more robust spinel phases at 167°C	⁴⁹ Rauwel et al. (2012)
Thermal ALD	Electrochromic devices, heterogeneous catalysts, solid state gas sensors, resistance random access memory (ReRAM) devices, intercalation compounds for energy storage, and active catalyst in air pollution control for reduction of NO _x , CO, and volatile organic compounds (VOCs)	Growth of a mixture of Co ₃ O ₄ and CoO phases from CCTBA (Co-003) in the temperature range of 68–138°C with no impurities detected	⁵⁰ Han et al. (2012)
Thermal ALD	IC and other devices	ALD Co achieved at low temperatures due to the high reactivity of the Co source precursors	⁵² Kalutarage et al. (2013)
No actual ALD deposition, only synthesis, structural, and chemical characterization of Co precursors, as well as solution reduction reactions	Seed layers for Cu metallization; capping layers for Cu lines; silicides as contact material in IC applications; magnetoresistive random access memory devices; catalytic applications	3 Co complexes: Co(tBuNNCHCtBuO) ₂ ; Co(tBuNNCHCtPrO) ₂ ; Co(tBuNNCMeCMeO) ₂	⁵³ Kalutarage et al. (2013)
Thermal and plasma ALD	Microelectronics technology; spintronics; giant magneto-resistance in read heads for hard disks; magnetoresistive random access memories (MRAMs); magnetic alloys; cutting-wear resistant alloys and super alloys	A review article of ALD precursor design and reaction mechanisms, including a summary of published work for Co thermal ALD and Co selective ALD	²⁰ Ramos et al. (2013)
Thermal ALD and plasma ALD	Seed layer for Cu metallization; IC source and drain contact materials; magneto-resistive random access memory devices	A review article of thermal ALD, including: (2-t-butylallyl)Co tricarbonyl (Co-108); Co(iPrNCMeNiPr) ₂ ; Co(C ₅ H ₅)(CO) ₂ (Co-103); Co(C ₅ H ₅) ₂ (Co-203); Co ₂ (CO) ₈ Co-001; Co(C ₅ H ₅)(iPrNCMeNiPr) (Co-207)	⁵⁴ Knisley et al (2013)
No actual ALD deposition. Only synthesis, structural, thermal, and chemical characterization of Co precursors	Seed layer for Cu metallization; magnetoresistive random access memories (MRAMs);	Co complex containing carbonyl ligands: C ₁₄ H ₃₀ CoN ₄ O ₂	³⁵ Karunarathne et al. (2013)
Thermal and Plasma-enhanced ALD (PE-ALD)	Contact material of nanoscale electronic devices	PE-ALD of Co from bis(η -methylcyclopentadienyl)Co(II) Co(MeCp) ₂ (Co-204) using NH ₃ or H ₂ plasma as co-reactant; comparative analysis of Co growth characteristics and film properties from ALD Co(MeCp) ₂ (Co-204) versus cobaltocene (Co-203) and cyclopentadienyl isopropylacetamidinato-Co (Co-207)	³⁶ Park et al. (2013)

Table V. (Continued).

Deposition Technique	Potential Applications	Brief Description	Reference
Plasma-enhanced ALD (PE-ALD)	As diffusion barrier and seed layer in IC Cu metallization	PE-ALD Co from dicobalt hexacarbonyl t-butylacetylene (Co-005) for Cu direct plating. Co film resistivity decreased when pre-treating TaN _x substrate with H ₂ plasma.	³⁷ Park et al. (2014)
Thermal ALD	As capping layer in IC Cu metallization	ALD Co films consisting of two layers: a polycrystalline Co phase on top of a Co-Cu phase	³⁸ Elko-Hansen et al. (2014)
Thermal ALD	Magnetic materials, CoSi ₂ , contact materials, and liners and caps of Cu features in IC devices	A 2-step Co ALD process that did not yield any Co films	³⁹ Klesko et al. (2016)
		A 3-step Co ALD process that involved the formation of intermediate Co(II) formate layers that were then reduced to Co metal, implying the utilization of bis(TMS)pyrazine as reducing agent.	³⁹ Klesko et al., supporting documentation to Reference 31 (2016)
No actual ALD deposition, only synthesis, thermal and chemical characterization of Co precursors	IC applications	Co complexes of the type [Co(NHC) ₂ (CO)(NO)] bearing N-heterocyclic carbenes (NHCs) based on the reactivity of NHCs with [Co(CO) ₃ (NO)] (Co-002)	⁴⁰ Hering et al. (2016)
Electrochemical ALD (e-ALD)	As a replacement for Cu interconnects in emerging IC devices	A two-step e-ALD process employs a Zn sacrificial layer that undergoes spontaneous surface-limited redox replacement by Co	²⁶ Venkatraman et al. (2017)
Plasma-enhanced ALD (PEALD)	Soft magnet phase of magnetically exchange coupled magnet consisting of hard and soft magnet phases	Co thin films with face-centered-cubic crystal structure that were not oxidized	⁴¹ You et al. (2018)
Hot-Wall Cross-Flow ALD Reactor	Liners and caps in IC Cu interconnects, as seed film for CoSi ₂ as IC contact material, and in magnetic memories	A two-step ALD process that deposits CoO which is then subjected to a reduction process in forming gas to yield Co	⁴² Väyrynen et al. (2018)
Shower head type ALD system	Amorphous metal alloys (metallic glasses) due to their uncommon properties, such as high hardness, soft magnetism and electrical behavior	Co and TiN were grown via cyclic combination of ALD to form multilayered Co/TiN stacked structures	⁴³ Nam (2018)
Thermal ALD Thermal Pulsed-MOCVD	Spintronic devices for nonvolatile magnetic random access memories (MRAM) and diluted magnetic semiconductors (DMS)	ALD and pulsed MOCVD were performed using a variety of co-reactants, with no self-limiting growth behavior observed. It was determined that the precursors studied could not be used as pure ALD precursors, and were more appropriate for low-temperature MOCVD Co films	⁴⁴ Lubitz et al. (2018)
Remote plasma ALD using a home-built reactor equipped with an inductively coupled plasma source	Magnetoresistive random access memory and CoSi ₂ contacts. Applications in IC interconnect technology, including liner for Cu interconnects, and replacement of Cu or W in small-dimension interconnects in IC front-end of the-line	3 different co-reactants were tested: NH ₃ , N ₂ +H ₂ mix, and N ₂ then H ₂ . NH _x species in the plasma were shown to play a key role in film composition, with higher NH _x concentration leading to purer films. It was therefore determined that H ₂ or N ₂ plasmas alone are not suitable as co-reactants. The authors argue that cobaltocene (Co-203) molecules chemisorb to the substrate surface, followed by the Cp rings reacting with surface H and being released as HCp to form Co, with the H provided from plasma NH _x species	⁴⁶ Vos et al. (2018)
Thermal ALD	N/A	An analysis of surface conversions in ALD reactions using reactions known in inorganic chemistry that are adjusted by applying relevant factors mandated by the lack of a solvent and the presence of surface ligands. The example given is 1,1-migratory insertion in Co(I) complex which reacts with H-terminated Si surface but not hydroxyl terminated Si surface	⁴⁷ Barry et al. (2018)

Table VI. Summary of Recent Area Selective ALD Cobalt Work.

Deposition Technique	Potential Applications	Brief Description	Reference
Area Selective Thermal ALD	GMR effect utilizing Co/Ru multilayers; nanomagnets; nanoscale semiconductor device fabrication such as nanocrystal memories; and IC contact material	Comparative study of thermal ALD Co using NH ₃ versus H ₂ as co-reactant, with the NH ₃ process yielding pure Co thin films with excellent conformality and nanoscale thickness controllability. The process was implemented in area-selective ALD employing octadecyltrichlorosilane self-assembled monolayer as a blocking layer to produce 3 μm wide Co line patterns without an etching process.	⁵⁹ Lee et al. (2010)
Experimental Area Selective Thermal ALD and theoretical calculations based on density functional theory (DFT)	GMR, spintronics, and IC technology; CoSi ₂	Co ALD selectivity demonstrated on H-terminated Si versus hydroxylated-SiO ₂ surface	⁶⁰ Kwon et al. (2012)
Area Selective Thermal ALD	Caps and liners for Cu metallization structures in IC devices	Co ALD for CoWP as capping layer for Cu interconnects	⁶¹ Elko-Hansen (2014)
Mechanistic and Growth Reactions for selective ALD Co	Nanoscale applications	Summary of Kwon et al. ⁶⁰ work on selective Co ALD	⁶² Elliott et al. (2016)
Area Selective Thermal ALD	Magnetic materials, intermediate layers in the fabrication of CoSi ₂ contacts, caps and liners for Cu metallization structures in IC devices, Cu replacement as conductor in future IC devices	Co metal selective growth was achieved on metallic (Pt, Ru, and Cu) but not insulating surfaces with specific co-reactants (butylamine and diethylamine) but not others (triethylamine); no growth was obtained on any other surface with any of the co-reactants Co metal selective growth was achieved on metals versus Si(100) and H-terminated Si; Co(II) formate was formed on SiO ₂ substrates, while carbon-doped oxide (CDO) substrates exhibited particle formation	⁶³ Kerrigan et al. (2017) ⁶⁴ Kerrigan et al. (2017)

growth occurring either in island mode, layer-by-layer (step) mode, or a combination of modes. Concomitant with or subsequent to adsorption, volatile reaction byproducts are released from the substrate surface. Substrate temperature plays a pivotal role in the deposition process:¹⁷ increased substrate temperature leads to longer surface diffusion distances, thus extending surface reaction times and potentially producing enhanced step coverage and reduced contaminant incorporation. However, Co film growth in thermal MOCVD proceeds as isolated islands or disconnected layers until a specific thickness is achieved which enables the islands or layers to connect and establish a continuous film.¹⁵ Because this characteristic is not conducive to the formation of extremely thin coherent layers, MOCVD Co is of limited utility in nanoscale device features. An additional challenge in MOCVD Co is that of achieving tight control of surface reactions in order to precisely control the thickness of extremely thin films by minimizing film growth rates.

Thermal Co ALD is categorized by: (1) the introduction of the Co source precursor and co-reactant in sequential rather than simultaneous stages, with intervening purge steps to ensure that the co-reactants never cross paths in the reaction zone and that no reactions occur except on the substrate surface; and (2) Co film growth proceeding through self-limiting surface reactions that ensure precise control of film thickness and conformality with atomic level accuracy.^{20,51-53} These characteristics suggest the realization of excellent film conformality in extremely aggressive device topographies. The addition of plasma to one of the co-reactants (e.g., H₂ or NH₃) has also been shown to enhance the ALD reaction and increase film growth rates by creating a higher concentration of active co-reactant radicals. Furthermore, the use of plasma to perform surface treatment between various ALD reaction steps leads to higher surface adsorption of Co precursor species by maximizing the concentration of active surface sites and decreasing reaction activation energy, thereby leading to lower deposition temperatures.^{36,51,54}

ALD exhibits a number of attractive features.^{26,37-41} In addition to enabling excellent conformality in nanoscale device topographies and feature sizes, ALD tends to grow particle and pin-hole free films while also providing excellent management of film thickness down to a few atoms. Another emerging advantage of thermal Co ALD is its ability to enable or prevent area-specific or area-selective film growth, in what is commonly referred to as area-selective ALD.⁵⁹⁻⁶⁴ Customized complexes (precursors) and surface assemblies or configurations can be made to react in a tightly controlled fashion so as to catalyze or inhibit Co deposition on specific areas of the underlying substrate surface, resulting in Co film formation only on the desired regions of the substrate. However, current ALD technologies suffer from high surface roughness and very limited growth rates (and thus low manufacturing throughput).

Reports have recently emerged on the development and application of pulsed Co MOCVD,^{6,20,44} the most widely accepted definition of which describes it as equivalent to thermal ALD, except that the process is performed at a substrate temperature leading to partial or complete decomposition of the pulsed Co precursor upon engagement with the substrate during every exposure cycle, rather than being limited to a simple physisorption or chemisorption reaction. The co-reactant is subsequently introduced to complete the decomposition reaction and/or remove the reaction byproducts, ensuring a clean Co film. Pulsed MOCVD can also be defined as equivalent to thermal MOCVD, except that the co-reactants are pulsed simultaneously into the reaction zone.

A synopsis of Co source chemistries is presented below, with particular attention given to the potential role of Co oxidation state in driving the chemical properties and associated decomposition pathways of the corresponding Co complexes. To this end, Table X outlines the Co-, C- and N- bond dissociation energies for appropriate Co source chemistries, while Tables XI displays pertinent properties of the recently considered thermal MOCVD, pulsed thermal MOCVD, and thermal, plasma and area-selective ALD. Finally, key processing parameters and major findings are presented in Tables VIII, IX and X

for thermal MOCVD, pulsed thermal MOCVD, and thermal, plasma and area-selective ALD, respectively, which are analyzed in detail in the relevant sections.

Modeling and Mechanistic Studies

Tables III presents a synopsis of several MOCVD and ALD Co theoretical and experimental modeling and mechanistic studies that shed light on the role of substrate surface and co-reactant chemistry in the adsorption and decomposition pathways of Co precursors and resulting film morphology, composition and properties.

Zaera et al.⁵ review the underlying mechanisms in thermal ALD and, although no ALD Co work is specifically discussed, present principles that are highly relevant to the subject of this review. In particular, the authors compare the role of semiconducting and insulating surfaces versus conducting surfaces in the precursor adsorption and decomposition process. They argue that precursor-substrate interactions are quite confined on semiconducting and insulating surfaces, where the electronic density is localized, involving specific atoms on the surface. In contrast, more complex precursor-substrate interactions are observed on metallic surfaces, where electronic density tends to be delocalized. In either case, however, precursor adsorption, decomposition and film growth appear to be initiated by specific reactive sites or lattice defects (nucleation centers) on the substrate surface. In the case of oxide substrates, for example, these reactive surface sites tend to be hydroxyl groups, with OH groups displacing precursor ligands and bonding through oxygen atoms to the remaining precursor structure. This coordination could take place with the H atom in the hydroxyl group being transferred to the displaced ligands, either concurrently, or subsequently to their removal. The degree of reactivity of these nucleation centers toward the ALD precursors could also be the reason for the ALD incubation delay or induction period that are reported during the first few cycles of the deposition process.

The review by Emslie et al.⁶ highlights the target requirements for the different classes of co-reactants used for metal ALD or pulsed MOCVD, and discusses the reaction pathways known or proposed to be involved in the corresponding ALD or pulsed MOCVD process. The authors argue that reactants must: (i) be sufficiently volatile to allow low-temperature ALD or pulsed MOCVD; (ii) have adequately high thermal stability to allow transport and delivery into the reaction zone while maintaining integrity; (iii) display reasonable reactivity with Co source precursor to enable ALD at substrate temperatures below the onset of MOCVD, and yield only volatile byproducts; (iv) have the ability to catalyze precursor reactions with substrate and Co film growth on both the initial substrate surface and the growing Co film. To this end, they emphasized two reports that analyzed and compared the role of ammonia (NH₃) versus dimethylhydrazine (N₂H₂Me₂) in the ALD and pulsed MOCVD growth of Co: (i) Co₂(amd^{ipr})₂(Co-206) with NH₃ on H-terminated Si or SiO₂ to grow Co metal at 350°C, in which the reaction appears to proceed through the formation of CoN as an intermediate which subsequently decomposes to Co at approximately 300°C (via Co₂N and Co₃N); (ii) t-Bu-allyl)Co(CO)₃ (Co-108) with dimethylhydrazine (N₂H₂Me₂) on H-terminated Si to grow Co at 140°C,⁶⁰ in which the low temperature precludes the formation of CoN as an intermediate, indicating that the reaction proceeds directly to the formation of Co metal.

Elliott et al.⁷ performed a multi-phase theoretical study of the underlying mechanisms in ALD Co from t-Bu-allyl)Co(CO)₃ (Co-108) and zero-valent Co complexes containing “non-innocent” ligands such as the diazadienyl molecules tBu₂DAD (Co-208) and Me₂DAD (C₄H₈N₂). Employing mechanistic information from density functional theory calculations for shortened cycles of precursor interactions with co-reactants such as H₂, the authors investigated how ligands can be cleanly eliminated to yield pure Co, as well as what effects side-reactions could have on the incorporation of impurities (such as C) and other unwanted products (such as CoO).

Phase I of this study explored the adsorption of t-Bu-allyl)Co(CO)₃ (Co-108) and selective deposition on H-terminated Si versus OH-

Table VII. Summary of Thermal MOCVD Cobalt Deposition Parameters and Related Data.

Reactor Type	Substrate	Sub. T (°C)	Precursor (Sublim. or vaporiz. T (°C))	Carrier gas	Co-reactant (Flow Rate, sccm)	Growth Rate (nm/min)	Duration of Deposit. (sec)	Working Pressure (torr)	Film Thick. (nm)	Pertinent Details	Reference
Custom-designed cold-wall CVD system	Si, SiO ₂ , SiN _x	210- 480	Cobalt tricarbonyl nitrosyl (Co-002) 5sccm@50°C	Ar	H ₂ (750)	~9nm/min	180–1800	1.5	~140nm	Optimum growth window for substrate T between 350–480°C. Films were metallic fcc Co with film resistivity between 8.5 μ cm and 11 μ cm. No O, C or N contaminants.	³ Ivanova et al. (1999); ¹³ Londergan et al. (2001)
Pulsed liquid injection thermal MOCVD (PI-MOCVD)	Mono-crystalline LaAlO ₃ (100) and Si(100)	450 and 600	Co(acac) ₂ (Co-201) and Co(thd) ₂ (TMEDA) in 1,2-dimethoxy- ethane (monoglyme)	Ar (900 sccm) + O ₂ (600 sccm)	None	Co(acac) ₂ : ~11.5nm/ min @ 450°C; ~26.5nm/ min @ 600°C. Co(thd) ₂ : ~8.5nm/ min @ 450°C; ~21.5nm/ min @ 600°C.	N/A	5	100–400	Epitaxial cubic Co ₃ O ₄ films were grown from both precursors on LaAlO ₃ substrates. Epitaxy attributed to lattice match and the presence of excess oxygen in reaction zone. Polycrystalline Co ₃ O ₄ films were grown from both precursors on Si substrates.	⁶⁷ Pasko et al. (2004)
Cold-wall MOCVD reactor equipped with pulsed-spray evaporation (PSE) precursor delivery	Bare glass Ni- coated glass SiC	325 (SiC) 240- 325 (bare glass and Ni coated glass)	Co(acac) ₂ (Co-201) dissolved in either ethanol or n-propanol and pulse-injected @ 40ms/ cycle	N ₂ @ 1000 sccm	None	~5nm/min on Ni coated glass	150–2400	110	5–120	Growth achieved on all substrates, with Ni surface yielding better Co morphology and eliminating ALD incubation period. Films were metallic Co or Co ₂ C, depending on selection of alcohol solution and substrate T. Isopropanol solution produced Co ₂ C at 205–230°C; n-propanol solution produced metallic Co at temperatures above 250°C.	⁸ Premkumar et al. (2007)
Standard MOCVD chamber	Co β-diketonate Co(acac) ₂ (Co-201). Inclusion complex of β-cyclodextrin with Co iodide (CoI ₂). No actual deposition work performed, only characterization of Cobalt β-diketonate Co(acac) ₂ Co-201 and inclusion complex of β-cyclodextrin with cobalt Iodide (CoI ₂) by XRD and Differential Thermal Analysis.										⁹ Papadopoulos et al. (2008)
Standard MOCVD chamber	B-doped p-type Si(100) Patterned wafers with SiO ₂ trench structures 0.12μm wide and 1.8 μm deep on Si	150	(dicobalt hexacarbonyl t-butylacetylene (Co-003) @20°C	Ar @ 20 sccm	H ₂	N/A	N/A	1–12	N/A	C and O content and film resistivity decreased with higher H ₂ partial pressure in reaction zone, from 15at% to 2.8at%, 5at% to 1at%, and 130 μ cm to 30 μ cm, respectively. Co films RTA annealed between 400 and 900°C in increments of 100°C under ambient N ₂ for 1 min. CoSi ₂ was formed above 600°C.	¹⁰ Lee et al. (2008)

Table VII. (Continued).

Reactor Type	Substrate	Sub. T (°C)	Precursor (Sublim. or vaporiz. T (°C))	Carrier gas	Co-reactant (Flow Rate, sccm)	Growth Rate (nm/min)	Duration of Deposit. (sec)	Working Pressure (torr)	Film Thick. (nm)	Pertinent Details	Reference
Cold-Wall Atmospheric Pressure MOCVD (AP-MOCVD) System	Si(400)	250, 275, 300, 325 and 350	Co(III) precursors of the general form: (η^5 -C ₅ H ₅)Co(R ₂ -dab) containing N,N ² -dialkyl diazabutadiene and N,N ² -diaryl diazabutadiene, or N,N ² -diaryl diazabutadiene, where R was as follows: isopropyl (Co-302) t-butyl (Co-303) cyclohexyl; 2,4,6-trimethyl phenyl; and 2,6-diisopropylphenyl. AP-MOCVD performed only with the isopropyl derivative CpCo(^t Pr ₂ -dab) (Co-302) maintained @130°C	H ₂ @ 700 sccm	H ₂	3.73nm/ min (325°C) 8.47nm/ min (350°C)	1800	760	112 (325°C) 254 (350°C)	Films grown above 325°C were coherent and pinhole free. Films grown below 325°C exhibited a crystalline nanoparticle morphology. Films were high purity metallic Co with no Co silicide at the interface with Si. C incorporation was detected >300°C, accompanied with an increase in sheet resistance.	¹⁷ Pugh et al. (2013)
Cold-wall chamber with vacuum sample transfer chamber	SiO ₂ (500 nm)/ Si substrate Electroplated Cu/PVD TaN/ Si wafer	90–350	dicobalt octacarbonyl (Co-001) as Co source. tungsten hexacarbonyl [W(CO) ₆] as W source. N/A	N/A	N/A	N/A	N/A	N/A	10–30 (Co-W alloy)	Co-W alloy thin films as diffusion barrier for Cu. Films grown above 50°C were Co, while films produced above 150°C were CoW _x alloys. Co film resistivity was as low as 10μ cm. CoW _x film resistivity increased with W content from 100μ cm @ 10%W to ~500μ cm @50% W. As W content increased from 10% to 30%, C and O contamination also increased from ~4at% and ~5at% to ~9at% and 25at%, respectively. Addition of W improved Cu barrier properties. CoW _x with 20% W had equivalent diffusion resistance to PVD Ta, though resistivity suffered.	³⁴ Shimizu et al. (2013)
Home-built vertical cold wall CVD reactor equipped with a continuous evaporation system	100 nm thick thermal SiO ₂ on Si	350	The Co ⁰ source Hexacarbonyl (trimethylsilylacetylene) (Co-004) precursor vaporized @ RT	N ₂ @ 50 sccm	None	N/A	N/A	N/A	70–80	The resulting films contained 68.5at% Co, 26.6at% O and 4.1at% C, and consisted of a mixture of Co and CoOx.	¹⁸ Georgi et al. (2013)

Table VII. (Continued).

Reactor Type	Substrate	Sub. T (°C)	Precursor (Sublim. or vaporiz. T (°C))	Carrier gas	Co-reactant (Flow Rate, sccm)	Growth Rate (nm/min)	Duration of Deposit. (sec)	Working Pressure (torr)	Film Thick. (nm)	Pertinent Details	Reference
		250–380	Dicobalt- tetrahydrides: low melting or liquid Co ⁽⁰⁾ precursors of type [Co ₂ (CO) ₆ (η ² -RC≡CR')] (R=H, R' = (CH ₃) ₃ Si, (Co-004) ⁿ C ₄ H ₉ , ⁿ C ₅ H ₁₁ , ⁿ C ₆ H ₁₃ , ⁿ C ₇ H ₁₅ ; R= ⁿ C ₃ H ₇ , CH ₃ ; R=R' = C ₂ H ₅ , (CH ₃) ₃ Si). Vapor pressure in the range of cobaltocene (Co-203) and Co ₂ (CO) ₈ (Co-001) all vaporized @RT			3.0–10.0	180–3600	0.2–37 torr	50–90	Of all precursors tested, only [Co ₂ (CO) ₆ (η ² -(CH ₃) ₃ Si)C≡C(CH ₃) ₃ Si] (Co-004) yielded films with 96.7at% Co and 2.5at% C. Films were deposited @250°C with no co-reactant @ a growth rate of 10nm/min. All other precursors yielded films with significant C and O contamination.	²⁹ Georgi et al. (2014)
			No actual deposition work: a follow up to the Shimizu et al. work above ³⁴ that examined the adhesion properties of Cu to Co-W alloys. Precursors used: hexafluoroacetylacetonato copper(I) trimethylvinylsilane (Cu(hfac)(tmvs)); octacarbonyldicobalt (Co ₂ (CO) ₈) (Co-001) and hexacarbonyl tungsten (W(CO) ₆) for Cu, Co and W, respectively. This work showed that adhesion of Cu increases as follows: PVD Cu/PVD Ta, CVD Cu/CVD Ta, then ALD Co(W). ALD Co(W) exhibited better Cu adhesion than CVD Co(W).								³⁰ Shima et al. (2014)
Vertical type MOCVD reactor	Si(111)	300–420	Bis (2-methylamino-4-methyliminato-penten)Co(II), Co(N ⁺ acN ⁺ ac) ₂ 120–130 (v.p. ~0.06 torr)	Ar @ 1000 scc per hour	H ₂ @ 4000 scc per hour	N/A	N/A	760	20–180	At precursor evaporation T = 120°C, Co content in the films decreased from 91.4at% @ substrate T = 310°C to 44.2at% @ substrate T = 420°C, while C content increased from 8.3at% to 55.7at%. At precursor evaporation T = 130°C, Co content in the films increased from 84.8at% @ substrate T = 300°C to 90.9at% @ substrate T = 340°C, while C content decreased from 14.2at% to 8.8at%	¹⁴ Dorovskikh et al. (2014)
Cyclic thermal MOCVD in a cold wall CVD chamber mounted on a cluster tool	Si wafers	~80–225	dicobalt octacarbonyl (Co-001) R.T.	Ar	None	1.5nm/s @80°C, increasing to 3nm/s @100°C and remaining constant until 175°C, then decreasing to ~1.8nm/s @225°C	N/A	200 mtorr	~17@ 75 cycles. Increases linearly with cycles up to nearly 80nm @400 cycles	Films above 125°C were >99.5at% Metallic Co with insignificant O content. Film resistivity was <20μ cm. MOCVD films were magnetically softer, smoother and less textured than their PVD counterparts.	¹⁵ Samal et al. (2014)
Cold-Wall thermal MOCVD reactor	Si wafers	200 650	CpCo(Co) ₂ (Co-103) at R.T.	Ar	O ₂	200°C: 0.1 400°C: 2.5 500°C: 9.4 600°C: 7.0 650°C: 5.0 (nm/min)	N/A	0.75 to 7.5 mtorr	200°C: 2 400°C: 50 500°C: 190 600°C: 140 650°C: 100	Films grown below 400°C substrate temperature are a mixture of metallic Co and CoO. Between 400°C and 600°C, films are CoO. Above 600°C, films are Co ₃ O ₄ spinel structure. At 2 mtorr and 10 mtorr O ₂ partial pressure, films are a mixture of metallic Co and CoO. At 15 mtorr O ₂ partial pressure, films are CoO with C contamination.	⁷⁵ Schmid et al. (2014)

Table VII. (Continued).

Reactor Type	Substrate	Sub. T (°C)	Precursor (Sublim. or vaporiz. T (°C))	Carrier gas	Co-reactant (Flow Rate, sccm)	Growth Rate (nm/min)	Duration of Deposit. (sec)	Working Pressure (torr)	Film Thick. (nm)	Pertinent Details	Reference
Cold-wall Reactor equipped with pulsed-spray evaporation (PSE) precursor delivery	Si(100)	310	97% Co(acac) ₂ (Co-201) Precursor dissolved in ethanol and pulse-injected @ 15ms/cycle.	None	None	None	1800	N/A	N/A	Distilled H ₂ O was added to precursor solution for a systematic study of H ₂ O influence on MOCVD process and varied from 0.0 vol% to 5.0 vol%. The addition of any H ₂ O concentration yielded a Co oxide phase.	³¹ Weiss et al. (2015)
Direct Liquid Injection (DLI) MOCVD system	N/A	200–240	Co(iPr-MeAMD) ₂ (Co-206) dissolved in tetradecane Direct Liquid Injection @ 5g/hour @RT into a vaporization chamber set @ 150° C	N ₂ @ 100 sccm	H ₂ + NH ₃ @ total combined flow of 200 sccm H ₂ /NH ₃ ratio varied from no NH ₃ to no H ₂	N/A	N/A	10	N/A	MOCVD using H ₂ yielded no deposition. Films grown with NH ₃ /H ₂ ratio of 1/9 produced fcc Co. Films grown with NH ₃ /H ₂ ratio ranging from 1/3 to 3 yielded mixture of fcc and hcp Co. Films grown with just NH ₃ were hcp Co ₃ N. Best resistivity (25μ cm) was achieved for films grown with NH ₃ /H ₂ ratio of 1.	³² Yang et al. (2015)
Home-built vertical cold-wall MOCVD reactor connected to a continuous evaporation system	SiO ₂ (100nm)/ Si		Co ⁺¹ half-sandwich complex: [Co(η ⁵ -C ₅ H ₅)(L)(L')] where L, L'= 1,5-hexadiene	N ₂	None						¹⁹ Georgi et al. (2015)
		480	[Co(η ⁵ -C ₅ H ₅)(1,5-hexadiene) ₂] @25–70	10-80 sccm		0	3600	~0.2–3.75		No deposition	
		480	[Co(η ⁵ -C ₅ H ₅)(P(OEt) ₃)(H ₂ C = CHSiMe ₃)] @ 25–150	10-80 sccm		0	3600	~0.2–3.75	0	No deposition	
		350	[Co(η ⁵ -C ₅ H ₅)(P(OEt) ₃) ₂] @25	50		2.7 nm/min	1800	~0.2	80	Films consisted of 45.3at% Co, 38.1at% O, 11.7at% P and 4.9at%C.	
Hot-wall reactor	Si(111)	325, 350, 375, and 400	Co(I) precursors based on cyclopentadienyl and diene ligands. 11 CpCo(diolefin) complexes studied. Only [(C ₅ H ₅)Co(η ⁴ -CH ₂ CHC(Me)CH ₂)] (Co-107) was MOCVD tested @85°C.	H ₂ @ 300 sccm	H ₂ @ 700sccm	N/A	1800	760	N/A	Films were highly-crystalline, high-purity metallic Co with no silicide phase at the film's interface with Si. O content decreased with higher substrate T, from 3.2at% @325°C to 0.3at% @ 400°C. Co ρ decreased from 32.4μ cm @325°C to 17.6μ cm @400°C. Films were highly-oriented fcc structure.	¹⁶ Hamilton et al. (2016)
Hot-Wall MOCVD System	SiO ₂ / Si(100)	250	Co(II) compounds with guanidinate ligands. C ₂₆ H ₆₄ CoN ₆ Si ₄ MOCVD tested.	N ₂	O ₂	N/A	3600	N/A	N/A	Films consisted of a stoichiometric Co ₃ O ₄ phase	³³ Zhang et al. (2018)

Table VIII. Summary of Pulsed MOCVD and ALD Cobalt Deposition Parameters and Related Data.

Substrate	Substrate Temp (°C)	Co Source	Co Source Pulse Duration(s)	Co-reactant (flow rate)	Co-reactant Pulse (s)	Purge Gas	Purge Pulse Dur. (s)	Plasma (Type)	Work. Press. (torr)	Film Thick. (nm)	Growth Rate (nm/ cycle)	Pertinent Details	Ref.
Soda lime Glass Single Crystal Si(100)	114–307	Co(thd) ₂ (Co-202) sublimed @109.5°C	0.25–3	Ozone (500sccm)	0.5–6	N ₂	0.25–3	None	1.35	4–940 nm	0.016–0.020	ALD-type growth of Co ₃ O ₄ established across the entire substrate T range. Octahedron-shaped morphology observed at low T. Cube-shaped morphology seen for films deposited on Si(100) high T.	⁴⁵ Klepper et al. (2007)
Soda lime Glass Single Crystal Si(111) Alumina Anodics	137 to 331°C	CoCp ₂ (Co-203)	0.5 to 5 sec (optimum: 3 sec)	Ozone	0.5 to 5 sec (optimum: 3 sec)	N/A	N/A	None	N/A	N/A	0.041 to 0.045 nm/cycle as a fct of substrate	0.041nm/cycle growth rate on Si(111) versus 0.045 nm/cycle on soda-lime glass. Higher growth rate attributed to placement of substrates in reactor. Abnormally large thickness gradients observed above 331°C, indicating MOCVD Type decomposition regime.	⁴⁸ Diskus et al. (2011)
Si(001) and SiO ₂	300°	CoCp ₂ (Co-203) @ 78°C Ar carrier gas @50sccm	3	N ₂ +H ₂ mix @ various flow rates	3		2	300W (N ₂ +H ₂ mix @ various flow rates)	N/A	N/A	0.02 to 0.06 as fct of substrate T (150°C to 450°C)	Films grown with pure H ₂ plasma had very high resistivity and high C content (attributed to the ineffectiveness of H ₂ plasma as reducing agent in comparison with NH ₃ plasma). Similar results observed with pure N ₂ plasma. Films grown with N ₂ +H ₂ plasma had resistivities ranging from ~23μ cm @ N ₂ /H ₂ = 10% down to ~20μ cm @ N ₂ /H ₂ = 33%, which increased with higher N ₂ /H ₂ flow rates to ~35μ cm (corresponding to the atomic ratio in NH ₃ molecule).	⁵¹ Yoon et al. (2011)

Table VIII. (Continued).

Substrate	Substrate Temp (°C)	Co Source	Co Source Pulse Duration(s)	Co-reactant (flow rate)	Co-reactant Pulse (s)	Purge Gas	Purge Pulse Dur. (s)	Plasma (Type)	Work. Press. (torr)	Film Thick. (nm)	Growth Rate (nm/ cycle)	Pertinent Details	Ref.
Si (111) γ -alumina nanoporous particles with sizes ranging from 20 to 100 μ m in diameter dispersed on glass substrate	167°	CoCp ₂ (Co-203)	3	Ozone	3	N/A	10	None	N/A	10 nm	0.053 nm/ cycle on Si	Annealing in air for 3 hours up to 1000°C was insufficient to stabilize the spinel structure. δ -alumina spinel superstructure to θ -alumina monoclinic structure occurs before the stabilization of the Co spinel phase.	⁴⁹ Rauwel et al. (2012)
Ru(5nm)/ SiO ₂ (100nm)/ Si	180°	Co(NO ^t butyl Me ⁱ Pr) ₂ sublimed @90°C. Melting point @ 98°C	20	BH ₃ (NHMe ₂)	1	N/A	5 sec after precursor. 10 sec after reactant	None	N/A	N/A	0.007 nm/cycle	Metallic Co was deposited	⁵² Kalutarage et al. (2013)
B-doped Si (100)	68– 138°C	CCTBA (Co-003) @50°C	N/A	Ozone	N/A	Ar	N/A	None	N/A	N/A	0.1–0.6 nm/cycle	Deposition below 80°C governed by ALD-type (self-limiting) regime. Deposition above 80°C governed by CVD-type regime. [O]/[Co] ratio in films ranged from 103 to 108 as fct of substrate T.	⁵⁰ Han et al. (2012)

Synthesis, structural and chemical characterization, and solution reduction of Co(tBuNNCHCtBuO)₂; Co(tBuNNCHCtPrO)₂; and Co(tBuNNCMeCMeO)₂. Compounds were assessed for potential as ALD Co precursors by sublimation, thermogravimetric analyses, solid state decomposition studies, and solution reactions with reducing reagents. Co(tBuNNCHCtBuO)₂ was observed to sublime at 120–125°C at 0.05 torr, while Co(tBuNNCHCtPrO)₂ and Co(tBuNNCMeCMeO)₂ sublime at 100–105°C at the same pressure. All compounds were volatile and exhibited decomposition temperatures of 273–308°C for Co(tBuNNCHCtPrO)₂; 241–278°C for Co(tBuNNCHCtPrO)₂; and 235–250°C for Co(tBuNNCHCtPrO)₂. Treatment of Co(tBuNNCHCtBuO)₂ in tetrahydrofuran with hydrazine, BH₃ complexes and LiAlH₄ led to rapid formation of Co metal.

⁵³Kalutarage et al. (2013)

Table VIII. (Continued).

Substrate	Substrate Temp (°C)	Co Source	Co Source Pulse Duration(s)	Co-reactant (flow rate)	Co-reactant Pulse (s)	Purge Gas	Purge Pulse Dur. (s)	Plasma (Type)	Work. Press. (torr)	Film Thick. (nm)	Growth Rate (nm/ cycle)	Pertinent Details	Ref.
N/A	350°	Co complex with amidinate ligands: namely, Bis(N,N-diisopropyl-acetamidinato)Co(II) (Co-206) in solid form	N/A	NH ₃ versus H ₂	N/A	N/A	N/A	None	N/A	N/A	N/A	Co films grown by ALD with NH ₃ were denser and had 4 times lower resistivity (~50 μm) than those deposited with H ₂ ^{59,65}	²⁰ Ramos et al. (2013)
	200–300	Co(AMD ^{iPr2})Cp (Co-206), where the replacement of one of the AMD ^{iPr2} with Cp yields a liquid precursor (Co-207) with higher volatility than [Co(AMD ^{iPr2}) ₂]		NH ₃ plasma				NH ₃ plasma				Higher resistivity (~200 μm) and significantly more C (30at%) than films deposited with Co(AMD ^{iPr2}) ₂ ⁵⁵	
SiO ₂	300°	Cp ₂ Co (Co-203) CpCo(CO) ₂ (Co-103)		NH ₃ versus H ₂				NH ₃ plasma				Yielded Co carbide ⁵¹	
SiO ₂	300°	Cp ₂ Co (Co-203) CpCo(CO) ₂ (Co-103) ⁵⁰		NH ₃ plasma versus H ₂ plasma				NH ₃ Plasma versus H ₂ plasma				H ₂ plasma produced films with 5–8at% C. Only NH ₃ plasma yielded pure Co ⁵¹	
N/A	N/A	Carbonyl-based Co complexes: dicobalt octacarbonyl (Co-001) and t-Bu-acetylene dicobalthexacarbonyl ⁴² (Co-003)		plasma				H ₂ plasma				Since CCTBA Co-003 decomposes at 101°C and dicobalt octacarbonyl Co-001 loses CO at room T, it is surmised that the growth mechanisms involve a significant CVD component ⁶⁰	

A review article of: thermal ALD of Co(iPrNCMeNiPr)₂ (Co-206) with H₂ as co-reactant to yield Co @ 350°C with the very low growth rate of 0.012nm/cycle, and thermal ALD of Co(iPrNCMeNiPr)₂ (Co-206) with H₂ as co-reactant to yield Co @ 300°C. The substrate temperatures are significantly higher than the precursor decomposition temperature of 215–225°C, which implies a CVD rather than true ALD growth mode. Plasma ALD of Co(C₅H₅)(CO)₂ (Co-103); Co(C₅H₅)₂ (Co-203); Co₂(CO)₈, and Co(C₅H₅)(iPrNCMeNiPr) (Co-207) with NH₃, H₂ and N₂ plasmas.⁴⁹ Growth temperatures ranged between 75 and 175°C, and growth rates of up to 0.15 nm/cycle were achieved.

⁵⁴Knisley et al. (2013)

Table VIII. (Continued).

Substrate	Substrate Temp (°C)	Co Source	Co Source Pulse Duration(s)	Co-reactant (flow rate)	Co-reactant Pulse (s)	Purge Gas	Purge Pulse Dur. (s)	Plasma (Type)	Work. Press. (torr)	Film Thick. (nm)	Growth Rate (nm/ cycle)	Pertinent Details	Ref.
Sublimation studies, thermal decomposition temperature analyses and thermogravimetric/differential thermal investigations showed that the Co complex containing carbohydrazide ligands $C_{14}H_{30}CoN_4O_2$ is highly volatile and has a very high solid state decomposition temperature; it is therefore promising for use as a Co ALD precursor. Sublimation temperature: 75°C; melting point: 137–140°C; solid state decomposition temperature: 245°C; % recovery: 97.7%; nonvolatile residue: 0.0%.													³⁵ Karunarathne et al. (2013)
Si(001) and SiO ₂	100–350	bis(η-methylcyclopentadienyl)Co(II) (Co-204) @56°C. cobaltocene (Co-203). cyclopentadienyl isopropyl acetamidinato-Co (Co-207).	3	NH ₃ @ 400sccm versus H ₂ @ 400sccm	6	N/A	1	300 W	N/A	N/A	@300°C: 0.05 for Co(MeCp) ₂ (Co-203) 0.048 for CoCp ₂ (Co-203) 0.1 for Co(CpAMD)	Four reactants: H ₂ , NH ₃ and their plasmas, were investigated for ALD Co using Co(MeCp) ₂ (Co-204) and CoCp ₂ (Co-203). Only NH ₃ plasma deposited Co metal on either Si or SiO ₂ . The presence of NH ₃ radicals is therefore critical to obtain Co metal. For Co(MeCp) ₂ (Co-204), Co film resistivity decreased from 8500μ cm @ 100°C to 31 μ cm @ 350°C. Also, a few % C were detected in films grown >300°C.	³⁶ Park et al. (2013)
3 nm-thick TaN _x on SiO ₂	100–250	dicobalt hexacarbonyl 'butylacetylene (Co-003)	5	H ₂ @ 50-100 sccm	4	N ₂ @ 100 sccm	10.0 for precursor purge 5.0 for co-reactant purge	200 W	50 mtorr	N/A	0.08	Optimized substrate temperature for ALD Co ranged from 120–200°C. Temperature >200°C produced CVD like growth mode. Film resistivity on untreated TaN _x was ~90μ cm for films thicker than 20nm due to high C content (>20at%). Co resistivity decreased for TaN _x pre-treated with H ₂ plasma @100W for 1 min. This was attributed to the role of H in the reduction of CCTBA, with pre-treatment leading to TaN _x surface hydrogenation and an associated increase in the density of active substrate surface sites.	³⁷ Park et al. (2014)

Table VIII. (Continued).

Substrate	Substrate Temp (°C)	Co Source	Co Source Pulse Duration(s)	Co-reactant (flow rate)	Co-reactant Pulse (s)	Purge Gas	Purge Pulse Dur. (s)	Plasma (Type)	Work. Press. (torr)	Film Thick. (nm)	Growth Rate (nm/ cycle)	Pertinent Details	Ref.
300nm mainly (111) poly-crystalline Cu On TaN on SiO ₂	265	bis(N-t-butyl-N -ethylpropionamidinato) Co(II) (Co-209) Ar carrier gas	2	H ₂	15	Ar	15	None		~1–16 nm	~0.004 nm/ cycle (250 cycles) to 0.0053 nm/ cycle (3000 cycles)	Films were dual layer, consisting of a Co layer on top of a Co-Cu transition layer as thick as the Co layer. Intermixing occurred by grain boundary diffusion of Cu through the Co matrix. Polycrystalline Co is a mixture of fcc and hcp phases.	³⁸ Elko- Hansen et al. (2014)
Si, SiO ₂ , and Si-H Ru(13nm)/ TaN(2nm)/ SiO ₂ (100 nm)/ Si	~180	bis(1,4-di-t-butyl-1,3-diazabutadienyl) Co(II) (Co-208)	1-6 (saturation ≥ 3.0)	Formic acid	Saturation >0.1s	N ₂	10.0	None		10–200 as fct. of # of cycles	0.095	No Deposition observed on Si, SiO ₂ and Si-H. Optimum processing parameters: Co source (5.0s), purge (10.0s), formic acid (0.2s), purge (10.0s). Co ρ ~ bulk ρ of 6.24 μ cm. Growth rate decreased >200°C due to desorption or thermal decomposition of Co source.	³⁹ Klesko et al. (2016)

Synthesis and characterization of NHC complexes of the types: [Co(NHC)₂(CO)(NO)], where NHC = *i*Pr₂Im, *n*Pr₂Im, Cy₂Im, Me₂Im, *i*Pr₂ImMe, Me₂ImMe, Me*i*PrIm, Me*r*BuIm, R₂Im = (1,3-dialkylimidazolin-2-ylidene) [Co(NHC)(CO)₂(NO)] where NHC = *i*Pr₂Im (Co-109), *n*Pr₂Im, Me₂Im, *i*Pr₂ImMe, Me₂ImMe, Me*i*PrIm, Me*r*BuIm. All the complexes are volatile, stable upon sublimation and prolonged storage in the gas phase, and can readily decompose at higher temperatures. The complexes [Co(NHC)₂(CO)(NO)] appear more stable toward thermal decomposition versus [Co(NHC)(CO)₂(NO)]. The authors conclude that these Co complexes exhibit potential for application as precursors in vapor deposition of Co thin films.

⁴⁰Hering et al. (2016)

Table VIII. (Continued).

Substrate	Substrate Temp (°C)	Co Source	Co Source Pulse Duration(s)	Co-reactant (flow rate)	Co-reactant Pulse (s)	Purge Gas	Purge Pulse Dur. (s)	Plasma (Type)	Work. Press. (torr)	Film Thick. (nm)	Growth Rate (nm/ cycle)	Pertinent Details	Ref.
PVD Ru substrate	RT	CoSO ₄ electrolyte at pH 6.5	60s cycle duration (not pulse)	N/A	N/A	N/A	N/A	N/A	N/A	N/A	N/A	A 2-step electrochemical ALD (e-ALD) process. Not standard thermal or plasma ALD.	²⁶ Venkatraman et al. (2017)
τ-MnAl thin films	150	Dicobalt hexacarbonyl t-butylacetylene (Co-003) @ 50°C (flow set at 20sccm)	5	H ₂ (20sccm)	5	N ₂ (40 sccm)	20.0	200W H ₂ As reducing agent	0.1	2–6	0.2	ALD Co was achieved	⁴¹ You et al. (2018)
Si(100) Soda lime glass substrates	225–300	CoCl ₂ (TMEDA) @ 170°C in N ₂ as carrier gas @ 400sccm	0.5–2.0	H ₂ O oxide then reduced (H ₂ /N ₂)	0.5–5.5	N ₂	1.0–3.0	None	7.5	Up to 50	0.02–0.04 as function of higher subs T	ALD CoO was obtained and CoO was reduced in 10% forming gas to yield Co at temperatures as low as 250°C.	⁴² Väyrynen et al. (2018)
p-type Si glass substrates	200	Co(AMD) ₂ (Co-209) as Co source @ 75°C TDMAT as Ti source @ 50°C 50sccm Ar carrier gas	4.0 12.0 (each)	NH ₃	8.0	Ar	N/A	None	N/A	30	0.02 (Co) 0.03 (TiN)	Thickness ratios of Co and TiN were set as 2:1, 1:1, 1:2 and 1:4; corresponding cycles were 30:1, 15:1, 7:1 and 4:1, respectively. For 2:1, Co(56at%), Ti(11at%), N(12at%), 8at%C and 13 at%O. For 1:1 Co(41at%) Ti(22at%), N(7at%), 9at%C and 18 at% O. For 1:2, Co(38at%), Ti(28at%), N(9at%) with 5at%C and 20 at% O. For 1:4 Co(22at%) Ti(30at%), N(9at%) 9at%C and 30at% O. Co/TiN ratio: 2:1 ~2.3/1 1:1 ~1.25/1 1:2 ~ 1:1 1:4 ~0.5/1 (Co diffused in TiN). Amorphous or nanocrystalline phase.	⁴³ Nam et al. (2018)

Table VIII. (Continued).

Substrate	Substrate Temp (°C)	Co Source	Co Source Pulse Duration(s)	Co-reactant (flow rate)	Co-reactant Pulse (s)	Purge Gas	Purge Pulse Dur. (s)	Plasma (Type)	Work. Press. (torr)	Film Thick. (nm)	Growth Rate (nm/ cycle)	Pertinent Details	Ref.
N/A	70–175 ALD Mode ALD	[Co(CO) ₂ (NO) (¹ Pr ₂ Im)] (Co-109) sublimed @45°C	5	Air (including oxidation)	30	Ar	30	None	N/A	N/A	N/A	In deposition T regime of 70–175°C, precursor did not show any self-limiting growth behavior and cannot be used as pure ALD precursor. Precursor is suitable for low-temperature CVD of Co-based films.	⁴⁴ Lubitz et al. (2018)
N/A	70–175 Pulsed CVD Mode	[Co(CO) ₂ (NO) (¹ Pr ₂ Im)] (Co-109) sublimed @45°C	5	No	0	Ar	30	None	N/A	20	N/A		
N/A	170–260 ALD Mode	[Co(CO)(NO) (¹ Pr ₂ Im) ₂] (Co-109) sublimed @155°C	5	Air (including oxidation)	30	Ar	30	None	N/A	N/A	N/A	No significant effect of co-reactant choice, which may suggest that deposition occurs via thermal decomposition of the precursor, and that precursor is suitable for low-temperature CVD of Co-based films.	
				Air (excluding oxidation)									
				H ₂ NH ₃ /H ₂ (1:1 ratio @100 sccm each)									
				Air (excluding oxidation) H ₂ (@ 200sccm) NH ₃ /H ₂ (1:1 ratio @100sccm each)									

Table VIII. (Continued).

Substrate	Substrate Temp (°C)	Co Source	Co Source Pulse Duration(s)	Co-reactant (flow rate)	Co-reactant Pulse (s)	Purge Gas	Purge Pulse Dur. (s)	Plasma (Type)	Work. Press. (torr)	Film Thick. (nm)	Growth Rate (nm/ cycle)	Pertinent Details	Ref.
N/A	170–260	[Co(CO)(NO) (¹ Pr ₂ Im) ₂] (Co-109) sublimed @95°C	5	No	30	Ar	30	None	N/A	N/A	N/A		⁴⁴ Lubitz et al. (2018)
N/A	140–250	[Co(CO)(NO) (¹ Pr ₂ Im)(PMe ₃)] (Co-110) sublimed @95°C	5	NH ₃ /H ₂ (1:1 ratio @100 sccm each)	30	Ar	30	None	N/A	N/A	N/A	The precursor did not show any self-limiting growth behavior and therefore cannot be used as a pure ALD precursor. The precursor is suitable for low-temperature CVD of Co-based films.	
N/A	140–250	[Co(CO)(NO) (¹ Pr ₂ Im)(PMe ₃)] (Co-110) sublimed @95°C	5	No	30	Ar	30	None	N/A	65-72nm on Ru	N/A		
N/A	200	[Co(CO)(NO) (ME ₂ Im) ₂] (Co-109) sublimed @140-170°C	10	H ₂	30	Ar	30	None	N/A	None	N/A	No deposition. Instead, precursor solidified, turned darker, and polymerized or structurally deteriorated by either ligand rearrangement or decomposition.	

Table VIII. (Continued).

Substrate	Substrate Temp (°C)	Co Source	Co Source Pulse Duration(s)	Co-reactant (flow rate)	Co-reactant Pulse (s)	Purge Gas	Purge Pulse Dur. (s)	Plasma (Type)	Work. Press. (torr)	Film Thick. (nm)	Growth Rate (nm/ cycle)	Pertinent Details	Ref.
N/A	200 Pulsed CVD Mode	Co(CO)(NO)(ME ₂ Im) ₂] (Co-109) sublimed @140-170°C	10	None	0	Ar	30	None	N/A	None	N/A		⁴⁴ Lubitz et al. (2018)
SiO ₂ (450nm)/ Si	300	CoCp ₂ (Co-203) @80°C Ar as carrier gas	6	NH ₃ plasma	11	Ar	3	100W	15	25	Composition: Co with 0.5at% O; 0.6at% C; 2.3at% N $\rho = 41\mu$ cm. Composition: Co with 1at% O; 0.7at% C; 2.8at% N $\rho = 42\mu$ cm. Additionally, with increasing H ₂ partial pressure (H ₂ /(H ₂ +N ₂) rising from 0.13 to 0.77), film ρ decreased from $>10^9\mu$ cm to 78 μ cm. O content decreased from 7at% to 0.2at%. N and C contents remained constant at ~9at% and ~4at%, respectively. Co with 10at% O; 7at% C; 8.4at% N, $\rho = 1000\mu$ cm		⁴⁶ Vos et al. (2018)
									13	25			
									7.5	44			
H-Si Hydroxyl- SiO ₂	N/A	t-butylallylcobalt(I) tricarbonyl (Co-108)		N ₂ then H ₂ plasma									⁴⁷ Barry et al. (2018)

The authors describe a 1,1-migratory insertion of the t-butylallylcobalt(I)tricarbonyl complex into a Si hydride surface "ligand." The t-butylallyl ligand is π -coordinated to the metal center in an η^3 configuration, whereas bonding of that ligand in both the intermediate and final products exhibits σ (η^1) and π (η^2) characteristics. The migratory insertion does not occur in the case of a hydroxyl terminated Si surface.

Table IX. Summary of Area Selective ALD Cobalt Deposition Parameters and Related Data.

Substrate	Subs. T (°C)	Co Source (Vapor Pressure, torr)	Co Source Pulse Duration (s)	Co-reactant (flow rate)	Co-reactant Pulse Duration (s)	Purge Gas	Purge Pulse (s)	Plasma (Type)	Work. Pres. (torr)	Film Thick. (nm)	Growth Rate nm/cycle	Pertinent Details	Reference
Thermal ALD: Si(001) and SiO ₂	350	Bis(N,N'-diisopropylacetamidinato)Co ^{II} (Co-206) @65°C Ar carrier gas @50sccm	3	NH ₃ @400sccm	Ranged from 1–5	Ar @ 50 sccm	1	None	N/A	N/A	N/A	Growth rate using H ₂ as co-reactant (0.043nm/cycle) was nearly double that for NH ₃ (0.026nm/cycle). Films grown using NH ₃ as co-reactant were metallic and pure Co with little to no N inclusion. This shows that NH ₃ is effective at breaking the precursor Co-N bonds. Films grown in H ₂ exhibited high oxidation levels. ρ using H ₂ as co-reactant (200 μ cm) was 4 times that of NH ₃ (50 μ cm). Conformality was ~100% for both H ₂ and NH ₃ , indicating a saturated ALD surface reaction consistent with growth rate saturation. Co	⁵⁹ Lee et al. (2010)
For area-selective ALD: patterned octadecyl-trichlorosilane (OTS) on SiO ₂				H ₂ @400sccm	1							grown using either co-reactant formed selectively on SiO ₂ but not on OTS, showing that OTS is effective at blocking Co ALD nucleation and growth.	
OH-terminated SiO ₂ surfaces H-terminated Si(111)	140	t-butylallyl Cobalt tricarbonyl (Co-108) @35°C N ₂ carrier gas (flow rate = 10 sccm, P ~ 20 mTorr)	2	Dimethylhydrazine (DMHz) @ 9torr vapor pressure	1	N ₂	N/A	None	N/A	N/A	N/A	Experimentally, (tBu-AllylCo(CO) ₃) (Co-108) was unexpectedly substantially more reactive with H-terminated Si than OH-terminated SiO ₂ . The authors' theoretical calculations also indicated that the difference in relative energies of the Si and SiO ₂ surface reactions is significant, and acts as foundation for the observed substrate selectivity of (tBu-AllylCo(CO) ₃) (Co-108) for Co ALD.	⁶⁰ Kwon et al. (2012)

A review article of selective thermal ALD using Co(tBuNCHCHNtBu)₂ with DMHz to yield Co @ 140°C. The process showed very high selectivity for growth on H-terminated Si over hydroxide-terminated SiO₂.

⁵⁴Knisley et al. (2013)

Table IX. (Continued).

Substrate	Subs. T (°C)	Co Source (Vapor Pressure, torr)	Co Source Pulse Duration (s)	Co-reactant (flow rate)	Co-reactant Pulse Duration (s)	Purge Gas	Purge Pulse (s)	Plasma (Type)	Work. Pres. (torr)	Film Thick. (nm)	Growth Rate nm/cycle	Pertinent Details	Reference
Cu, SiO ₂ , and porous low-k ($k \sim 2.6$) dielectric carbon-doped oxide (CDO) Patterned line-spaced wafers	265	bis(N-t-butyl-N'-ethylpropionamidinato) Co(II) (Co-209) @ 80°C Delivered with 50sccm Ar	2	H ₂	15	Ar	15	None	260 mtorr	2.4-3	0.0048 (500 cycles) 0.003nm per cycle (1000 cycles)	Adsorption studies show that Co growth occurs most and least preferentially on Cu and CDO, respectively. They also indicate that CoAMD (Co-209), like other amidinate precursors, readily dissociates on transition metal surfaces such as Cu via a complex dissociative chemisorption mechanism. Extended trimethylchlorosilane (TMCS) exposures led to Co surface selectivity on Cu rather than on CDO. The ultimate per-cycle coverage on Cu is ALD-like and self-limited by the slow desorption of amidinate ligands and fragments from the Cu surface. Significant Cu-Co intermixing was observed by grain boundary diffusion of Cu through the Co matrix. C and N contamination was also detected in the Co films. In the case of SiO ₂ and CDO surfaces, the adsorption of CoAMD (Co-209) appears to be driven by interactions with exposed OH moieties. Both SiO ₂ and CDO favored the formation of oxidized Co ²⁺ and possibly Co ³⁺ species, as well as some partially reacted CoAMD precursor.	⁶¹ Elko-Hansen (2014)
N/A	> 150	tBu-AllylCo(CO) ₃ (Co-108)		1,1-dimethylhydrazine				None				Summary of the work of Lee et al.: ⁵⁹ Co growth reaction proceeds through the adsorption of t-butylallylCo(CO) ₃ (Co-108) to the H terminated Si surface (but not hydroxyl terminated SiO ₂ surface) without immediate ligand removal. This is followed by elimination of the allyl ligand by the surface H and subsequent formation of a Si-Co bond, leading to selective Co growth on Si but not on SiO ₂ .	⁵⁴ Knisley et al. (2013)

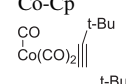
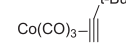
Table IX. (Continued).

Substrate	Subs. T (°C)	Co Source (Vapor Pressure, torr)	Co Source Pulse Duration (s)	Co-reactant (flow rate)	Co-reactant Pulse Duration (s)	Purge Gas	Purge Pulse (s)	Plasma (Type)	Work. Pres. (torr)	Film Thick. (nm)	Growth Rate nm/cycle	Pertinent Details	Reference
OH-terminated SiO ₂ , H-terminated Si(111)												Summary of the work of Kwon et al. ⁶⁰ on selective ALD Co from t-butylallylcobalt tricarbonyl (Co-108) and DMHz, emphasizing that the decomposition reaction proceeds selectively on H-terminated Si surfaces rather than on OH-terminated SiO ₂ . This is attributed to the donation of a Hydride rather than an H+ from the substrate to Co, with the nucleation reaction being thermodynamically favored on Si-H but not on SiO ₂ -OH.	⁶² Elliott et al. (2016)
Pt	200	Bis(1,4-di-t-butyl-1,3-diazadienyl)Co; (Co-208)	Varied	t-butylamine	0.2	N ₂	10	None	N/A	~20	0.098	Self-limited growth observed for precursor pulse >3.0sec and co-reactant pulse >0.1sec	⁶³ Kerrigan et al. (2017)
Cu, Ru, Pt			4.0							Varied as fct. of substrate	Varied as fct. of substrate	Self-limited growth occurs spontaneously on Cu and Pt substrates for 25–500 cycles. Normal growth on Pt after 200 cycles, with the delay attributed to oxidized surfaces present on Ru	
Si(100) with native oxide, thermal SiO ₂ , H ₂ terminated Si, and C-doped oxide substrates			4.0							0	0	No growth occurred	
Patterned substrates consisting of Si(100) substrates that contained a single, 1000 nm wide by about 60–80nm thick Pt stripe that was deposited by PVD using a shadow mask			4.0							0	0	After 1000 cycles, Pt stripe showed 47–51% Co and 49–53% Pt. The Si(100) region showed 1.1–1.6% Co and 0.2–0.3% PT, with the remainder comprising Si. The authors argue that small amounts of Pt may have diffused from the stripe onto the Si(100) during the ALD experiment, causing the seeding of small amounts of Co.	
Pt, Si(100) with native oxide, thermal SiO ₂ , H terminated Si and CDO substrates			4.0	diethylamine	0.2	N ₂	10	None	N/A	~20	0.098 on Pt ⁰ on insulating substrates	Growth characteristics in case of diethylamine were similar to tert-butylamine. Growth occurred on Pt but not on Si(100) with native oxide, thermal SiO ₂ , H terminated silicon and CDO substrates.	

Table IX. (Continued).

Substrate	Subs. T (°C)	Co Source (Vapor Pressure, torr)	Co Source Pulse Duration (s)	Co-reactant (flow rate)	Co-reactant Pulse Duration (s)	Purge Gas	Purge Pulse (s)	Plasma (Type)	Work. Pres. (torr)	Film Thick. (nm)	Growth Rate nm/cycle	Pertinent Details	Reference
Pt, Si(100) with native oxide, thermal SiO ₂ , H terminated Si and CDO substrates			4.0	triethylamine	0.2	N ₂	10	None	N/A	0	0	No growth observed in case of triethylamine on any substrate	⁶⁴ Kerrigan et al. (2017)
Ru (1nm)/ TaN (2nm)/ SiO ₂ (100nm)/ Si(100), Cu (33nm)/ TaN (7nm)/ SiO ₂ (100nm)/ Si(100), Pt (10nm)/ SiO ₂ (100nm)/ Si(100)	180	Bis(1,4-di-t-butyl-1,3-diazadieny)Co; (Co-208) @ 130°C	5.0	Formic acid	0.2	N ₂	10.0	None	6–9	2.5–25	0.095nm/min	Normal ALD growth @0.095nm/min occurs on Pt and Cu surfaces even within 25 deposition cycles. Growth was delayed on Ru surfaces until 100 cycles, then growth at very low growth rates until 250 cycles, when normal ALD growth @0.095nm/min was obtained. This indicates a nucleation delay on Ru until surface treatment with formic acid exposes active surface nucleation sites. Once the ruthenium surface is covered by a cobalt layer (150-250 cycles), normal self-limited ALD growth begins. On all conductive surfaces, Co films were metallic with resistivities in the range of ~15-20μ cm.	
Si(100) with native oxide, Si-H and CDO (30-50nm)/ SiO ₂ (100nm)/ Si(100)										0	0	No film growth was observed on Si(100), Si-H or CDO substrates	
Thermal SiO ₂ (100nm)/ Si(100)										35		Films were non-conductive and did not show the metallic texture of Co metal films. Analyses indicated the formation of Co(II) formate on the SiO ₂ surface.	
Si(100) with native oxide, Si-H and CDO (30-50nm)/ SiO ₂ (100nm)/ Si(100)	160, 170, 180, 190, 200, and 220									Equiv. of 25nm on metallic substrates		Depositions were performed at 160, 170, 180, 190, 200 and 220°C to observe the temperature at which nucleation starts to occur and determine the “area-selective ALD temperature” window. No deposition was observed up to 200°C. At 220°C, formation of particles was observed on CDO but not on Si(100) with native oxide or on Si-H.	

Table X. Cobalt-, Silicon-, Carbon- and Nitrogen- Bond Dissociation Energies for Selected Cobalt Source Chemistries.*

Source Precursor		Bond Dissociation Energy (kJ/mole)	Reference
N			
NH ₃	NH ₂ -H	435	76
	NH-H	377	
	N-H	314	
H ₂ NNH ₂	NH ₂ -NH ₂	297	
Si			
SiH ₄	H ₃ Si-H	396	77,78
	H ₂ Si-H	383	
	HSi-H	352	
	Si-H	293	
H ₃ SiSiH ₃	H ₃ Si-SiH ₃	310	
Co			
Co ₂ (CO) ₈ (Co-001)	(CO) ₄ Co-Co(CO) ₄	79±8	79
Co(CO) ₄ H (Co-101)	(CO) ₄ Co-H	243	79
Co(CO) ₃ NO (Co-002)	Co(CO) ₃ -NO	90	80
	Co(CO) ₂ NO-CO	-35	80
CpCo(CO) ₂ (Co-103)	CpCo(CO)-CO	184	81
	Co(CO) ₂ -Cp	327±2.89	81,82
Cp ₂ Co (Co-203)	CpCo-Cp	341.6	83
	Co-Cp	267.3	83
CCTBA (Co-003)		66	84
		5.8	84

*The table is intended to provide baseline comparisons of bond dissociation energies of selected Co, Si, C and N chemistries with some common precursors.

terminated SiO₂ surfaces, and determined that electron-rich substrate surface sites are needed for precursor adsorption; such sites potentially comprise metals, sub-oxides or reducing agents such as a hydride anion. Substrate surfaces that can act as H⁻ (hydride, not H⁺) donors to Co to catalyze precursor attachment, decomposition and Co nucleation include H-Si but not OH-SiO₂. This explains why the nucleation reaction is thermodynamically favorable on Si-H but not on SiO₂-OH surfaces—a phenomenon attributed to the distinct H-donor abilities of the former—as well as the resulting area-selective deposition observed on Si but not on SiO₂.

Phase II introduced H₂ as a co-reactant and examined its effects as a reducing agent. Since H₂ can act as both a proton and hydride donor, it could be applied simultaneously to both remove precursor ligands from the substrate surface and act as a reducing agent for the Co metal center. The authors refer to this as reductive elimination of ligands by hydrogenation.⁸ However, H₂ dissociation to yield either atomic radicals or the hydride anion is energetically favorable both at high temperatures, through the application of a plasma, and/or on substrate surfaces that enable such dissociative reaction. In any case, molecular H₂ can act effectively to reduce oxide-covered surfaces. In the case of ALD cobalt, since cobalt hydride is unstable, the role of hydrogen is limited to the first precursor exposure step and ends when precursor ligands are removed and the substrate surface is covered with cobalt in what Elliott et al. refer to as an “abbreviated cycle.” At the next exposure step, the precursor undergoes molecular or dissociative adsorption onto the bare cobalt surface, leaving the latter quite vulnerable to the incorporation of gas phase or precursor ligand contaminants such as O. Growth rates are also appreciably limited in this case.

Phase III analyzed co-reactants, one of which came from a family of reducing co-reactants where the hydride is bound to a metal or semi-metal center, such as hydrosilanes, hydroboranes, and hydroalanes. Unlike H₂, the benefit of these reagents is their ability to continue to

adsorb and yield a hydride-covered cobalt surface even after the first cycle of ligand removal and cobalt deposition. The resulting precursor reduction process with every exposure cycle should, in principle, lead to the deposition of pure cobalt void of impurities. These hydrides also have the advantage of promoting a significantly higher growth rate than that achieved in the case of the abbreviated cycle discussed above, in which the growth rate is limited by the instability of cobalt hydride.

Elliott et al. also discuss the potential of zero-valent cobalt precursors as attractive sources for Co CVD, arguing that, since the Co source precursor would not necessitate reduction, the role of the co-reactants would simply be to eliminate ligands via an oxidation process—similarly to ALD using an O₂-plasma to grow oxides. They further hypothesize that ligand oxidation would not produce transient OH species on the substrate surface, and conclude that Brønsted acidic amines may be viable co-reactants for zero-valent cobalt precursors.

Metal-Organic Chemical Vapor Deposition (MOCVD)

Tables IV and VII present a synopsis of thermal MOCVD Co applications, processing parameters, post-processing treatments (where applicable) and pertinent findings. A review of Tables IV and VII shows the following common trends in recent MOCVD work:

MOCVD Co films are employed as contact material in MOS field effect transistors (MOSFET) in conventional IC applications such as CoSi₂, as a diffusion barrier for Cu in multilevel metallization schemes, as effective adhesion layers (Co or Co-based alloys) in Cu interconnects, and as a wetting layer to induce void-free filling of narrow copper lines by reflow of nonconformal Cu. There are also several emerging uses for MOCVD Co films related to the Co magnetic dipole moment, such as spintronic and GMR devices and spin valves. MOCVD Co nanostructures are also applied as active materials in sensors, reflective and refractive coatings for optical devices, seed material for the growth of carbon nanotubes, as catalysts for self-aligned nanowires and in the Fischer-Tropsch (FT) process. Finally, MOCVD Co continues to be incorporated more widely as antibacterial, decorative, protective and wear-resistant coating.

Cold-wall and hot-wall thermal MOCVD processes appear to be the exclusive methods for cobalt deposition. No plasma activation or enhancement of any kind was used, perhaps due to concerns over the incorporation of contaminants into the resulting Co films. Various cobalt precursors with oxidation states ranging from 0 to 2 were utilized with a substrate temperature in the range of 80–480°C, with most processes reportedly occurring between 225°C and 350°C. Co-reactants included H₂, NH₃, (H₂+NH₃) mixture and oxygen (O₂), while carrier gases were primarily inert—namely argon (Ar) or nitrogen (N₂)—though a limited number of reports employed H₂. Noteworthy investigations and associated findings are discussed below.

Significant research activities have explored the development of new MOCVD precursor transport and supply methods to the reaction zone. Innovative precursor delivery techniques include: (i) pulsed liquid injection (PLI)⁶⁷ or pulsed-spray evaporation (PSE),^{8,31} (ii) continuous evaporation;^{18,19} (iii) direct liquid evaporation (DLE).³²

- In the PSE approach, the precursor, which is typically in solid form, is dissolved in a solvent and pulse-injected into the reactor at a predetermined frequency. Examples include a mixture of (0.05M) Co(thd)₂ and 1,2-dimethoxyethane (monoglyme) which was pulse-injected at a frequency of 2Hz; Co(acac)₂ (Co-201) which was dissolved in ethanol and pulsed-injected at frequencies ranging from 15ms/cycle³¹ to 40ms/cycle.⁸

- Continuous evaporation is a method based on the incorporation of a vaporizer unit that supplies a constant and controlled flow of a Co^(o) precursor / carrier gas mixture into the MOCVD reactor.¹⁸ The selection of low melting temperature or liquid Co^(o)

precursors of the type $[\text{Co}_2(\text{CO})_6(\eta^2\text{-RC}\equiv\text{CR}')]]$ ($\text{R}=\text{H}$, $\text{R}'=(\text{CH}_3)_3\text{Si}$ (Co-004), ${}^n\text{C}_4\text{H}_9$, ${}^n\text{C}_5\text{H}_{11}$, ${}^n\text{C}_6\text{H}_{13}$, ${}^n\text{C}_7\text{H}_{15}$; $\text{R}={}^n\text{C}_3\text{H}_7$, $\text{R}'=(\text{CH}_3)_3\text{Si}$, CH_3 ; $\text{R}=\text{R}'=\text{C}_2\text{H}_5$, $(\text{CH}_3)_3\text{Si}$); and $\text{R}={}^n\text{C}_3\text{H}_7$, $\text{R}'=(\text{CH}_3)_3\text{Si}$, CH_3 ; $\text{R}=\text{R}'=\text{C}_2\text{H}_5$, $(\text{CH}_3)_3\text{Si}$) allows the vaporizer to be maintained at room temperature.¹⁹

- In direct liquid evaporation, a precursor solution is vaporized by flowing it through a hot coil placed inside an oven, exploiting the almost instantaneous heat exchange between the heated solid loop and the liquid mixture to evaporate and deliver both the precursor and carrier gas efficiently and controllably to the reaction zone. The design and size of the tube force any non-volatile byproducts of the vaporization process to adhere to the bottom of the tube instead of contaminating the reactor, while the diameter of the tube orifice into the reactor prevents any clogging or blockage. In one embodiment, bis($\text{N,N}'$ -diisopropylacetamidinato)Co^(II) (Co-206) was dissolved in tetradecane and injected through a vaporization chamber set at 150°C.

All these delivery techniques share common advantages that include precursor storage at room temperature, which minimizes any thermally-induced decomposition effects resulting from long-term storage in a heated traditional bubbler as well as the ability to accurately and effectively control precursor flow rate into the MOCVD reactor.

A number of studies have also examined the role of additives in precursor decomposition mechanisms and the resulting Co film morphology and properties. For instance, Premkumar et al.⁸ compared the effects of isopropanol and n-propanol in MOCVD Co from Co(acac)₂ (Co-201), determining that the former yielded Co₂C at substrate temperatures in the range of 205–230°C, while the latter produced metallic Co at temperatures above 250°C. Weiss et al.³¹ examined the addition of water to a solution of Co(acac)₂ (Co-201) in ethanol to investigate the effects of humidity on precursor stability and MOCVD performance, concluding that water inclusion at any concentration led to the growth of a Co oxide phase.

Similar to the early MOCVD work by Ivanova et al.³ that yielded pure metallic Co from the source precursor cobalt tricarbonyl nitrosyl (Co-002), investigators have reported the growth of pure metallic cobalt from a number of cobalt sources, including:

- Dicobalt hexacarbonyl t-butylacetylene (Co-003) with H₂ as co-reactant at a substrate temperature of 150°C (Co oxidation state: 0; key parameter: high H₂ partial pressure in the reaction zone).¹⁰
- Isopropyl derivative CpCo(ⁱPr₂-dab) (Co-302) with H₂ as co-reactant at a substrate temperature above 325°C (Co oxidation state: 3; key parameter: substrate temperature).¹⁷
- Dicobalt hexacarbonyl bis(trimethylsilyl)acetylene (Co-005) with no co-reactant at a substrate temperature above 250°C (Co oxidation state: 0; key parameters: type of precursor and substrate temperature).²⁹
- Dicobalt octacarbonyl [Co₂(CO)₈] (Co-001) with no co-reactant at a substrate temperature above 125°C (Co oxidation state: 0; key parameter: substrate temperature).¹⁵
- Bis($\text{N,N}'$ -diisopropylacetamidinato)cobalt(II) (Co-206) dissolved in tetradecane with (NH₃ + H₂) mixture at a ratio of 1:1 and a substrate temperature in the range 200–240°C (Co oxidation state: 2; key parameter: NH₃/H₂ ratio).³²
- Co precursor based on cyclopentadienyl and diene ligands [(C₅H₅)Co(η⁴-CH₂CHC(Me)CH₂)] with H₂ as co-reactant at a substrate temperature of 400°C (Co oxidation state: 1; key parameter: substrate temperature).¹⁶

Co-W alloy thin films were also deposited by MOCVD from the co-reaction of dicobalt octacarbonyl (Co-001) and tungsten hexacarbonyl [W(CO)₆] as Co and W sources, respectively. The resulting alloys were then tested as a diffusion barrier in IC Cu metallization,³⁴ and the addition of W was shown to improve the barrier properties of the resulting CoW films against Cu diffusion. In particular, the addition of 20at% W to the Co matrix produced diffusion resistance behavior

equivalent to physical vapor deposition (PVD) Ta. However, film resistivity was significantly higher than metallic Co.

Atomic Layer Deposition (ALD) and Pulsed MOCVD

Tables V and VIII present a synopsis of pulsed MOCVD and ALD Co applications, processing parameters, post-processing treatments (where applicable) and pertinent findings. A review of Tables V and VIII shows the following common trends in recent pulsed MOCVD and ALD work:

Pulsed MOCVD and ALD Co films are also proposed for applications in traditional IC products, including as capping, adhesion and diffusion barrier layers in Cu interconnect structures, and as seed layers to catalyze Cu electroplating; CoSi₂ as contact material in Si transistors, and as a replacement for Cu interconnects in emerging nanoscale IC devices. New usages are also being explored that exploit cobalt's magnetic dipole moment, such as the soft magnet phase of magnetically exchanged coupled magnets consisting of hard and soft magnetic phases, non-volatile magneto-resistive random access memories (MRAMs), GMR devices and spin valves, and magnetic alloys. Additional applications encompass cutting-wear resistant alloys and super alloys, as well as amorphous metal alloys, also referred to as metallic glasses due to their special features such as high hardness and unique electrical properties.

Cold-wall and hot-wall thermal and plasma-enhanced ALD and pulsed MOCVD processes were all investigated for cobalt deposition. Various cobalt precursors with oxidation states ranging from 0 to 3 were utilized with substrate temperatures in the range of 70–350°C, with most processes reported occurring between 150°C and 350°C. Co-reactants included H₂, NH₃, (H₂+NH₃) mixture and forming gas (H₂/N₂), while carrier gases consisted primarily of inert gases, namely argon (Ar) or nitrogen (N₂), with a limited number of reports employing H₂. Exotic ALD methods to Co deposition included liquid phase (electroplating) in what the authors referred to as electroplating ALD (e-ALD), and two-step ALD involving the growth of CoO which was then reduced in forming gas to Co metal. Noteworthy investigations and associated findings are discussed below.

Significant plasma-enhanced (PE-ALD) research activities examined the role of plasma-activated co-reactants in the adsorption, reaction and decomposition of Co source precursors to yield metallic Co. Metallic Co was reported by a number of investigators from various Co sources, including:

- CoCp₂ (Co-203) with a (N₂+H₂) plasma at 300°C; a N₂/H₂ flow ratio of 33% produced metallic Co with the lowest resistivity (20μ cm). The authors point out that this percentage corresponds to the atomic ratio in NH₃ molecule and argue for the importance of NH₃ radicals in the clean cleavage of CoCp₂ (Co-203) to yield Co.⁵¹ The same finding was reported with CpCo(CO)₂ Co-103 and NH₃ versus H₂ plasma; the latter produced Co films with C contamination, while the former yielded pure Co at 300°C.^{20,51}
- Co(MeCp)₂ (Co-204) and CoCp₂ (Co-203) were both tested with NH₃ versus H₂ plasma at 100–350°C,³⁶ with only NH₃ plasma depositing Co metal. The investigators concluded that the presence of NH₃ radicals is critical to obtain Co metal, which is consistent with other reported results.^{20,46,51}
- Dicobalt hexacarbonyl t-butylacetylene (Co-003) in an H₂ plasma at 150°C.⁴¹

A number of thermal ALD studies investigated the role of co-reactants in the adsorption, reaction and decomposition of Co source precursors to yield metallic cobalt. Metallic Co was reported by a number of investigators from the following Co sources:

- Bis(N,N -diisopropylacetamidinato)Co^(II) (Co-206) with NH₃ versus H₂ as co-reactants at 300°C. Co films grown by ALD with NH₃ as co-reactant were denser and exhibited 4 times lower resistivity (~50μ cm) than those deposited with H₂. This finding appears to be consistent with the results reported by other investigators for PE-ALD using CoCp₂ (Co-203) as Co source precursor.^{20,65,66}

- Bis(1,4-di-*t*-butyl-1,3-diazabutadienyl)Co(II) (Co-208) with forming gas as co-reactant at 180°C.³⁹

Some ALD studies yielded metallic cobalt but in a growth regime that involved a significant MOCVD component. These Co source precursors would therefore qualify for pulsed MOCVD instead:

- Co(iPrNCMeNiPr)₂ (Co-206) with H₂ as co-reactant at 300–350°C to yield metallic Co. The substrate temperatures are significantly higher than the precursor decomposition temperature of 215–225°C, however, indicating a CVD rather than true ALD growth mode.^{56,57}

- Carbonyl-based Co complexes: dicobalt octacarbonyl³⁷ (Co-001) and *t*-Bu-acetylene dicobalt hexacarbonyl (Co-003) in H₂ plasma.^{37,60} Since CCTBA decomposes at 101°C and dicobalt octacarbonyl (Co-001) loses CO at room temperature, the authors surmised that the growth mechanisms involved a significant CVD component.

- [Co(CO)₂(NO)(ⁱPr₂Im)] (Co-109), [Co(CO)(NO)(ⁱPr₂Im)PMe₃], and [Co(CO)(NO)(ⁱPr₂Im)(PMe₃)] were all explored with Ar as co-reactant at substrate temperatures in the range 70–175°C.⁴⁴ The authors reported that the precursors did not show any self-limiting growth behavior and therefore cannot be used as strictly ALD precursors, but concluded that the precursors are suitable for low-temperature CVD of Co films.

Reports worth noting in light of their unique and innovative approach to the growth of metallic Co include:

- An electrochemical ALD (e-ALD) process that employed a 2-step approach based on a CoSO₄ electrolyte at a pH of 6.5. In a first step, underpotential deposition (UPD) is applied to grow a zinc (Zn) seed layer on a ruthenium (Ru) substrate; the sacrificial Zn layer is then subjected to spontaneous surface-limited redox replacement (SLRR) by Co to yield metallic Co.²⁶

- ALD CoO was obtained from the ALD reaction of CoCl₂ (TMEDA) and H₂O as co-reactant at substrate temperatures in the range 225–300°C. The CoO layer was then subjected to a reduction process in 10% forming gas (H₂/N₂) to yield Co beginning at temperatures as low as 250°C.⁴²

Area-Selective ALD

Tables VI and IX present a synopsis of area-selective ALD Co applications, processing parameters, post-processing treatments (where applicable) and pertinent findings. A review of Tables VI and IX shows the following common trends in recent area-selective ALD work:

Area-selective ALD Co films are being explored exclusively for conventional and unconventional IC applications. Traditional applications include CoSi₂ as contact material in MOS field effect transistors (MOSFET), as well as capping, seed, adhesion and diffusion barrier layers for Cu in multilevel metallization schemes. Emerging usages exploit cobalt's magnetic dipole moment for incorporation in spintronic and GMR devices and spin valves. The primary benefit of area-selective ALD Co is its potential to eliminate a number of the steps involved in conventional IC patterning and etching technologies, leading to an appreciable increase in manufacturing throughput and a significant reduction in cost of ownership.

Cold-wall thermal ALD processes are the exclusive methods for area-selective cobalt deposition. Due to the critical role that the substrate surface plays in the selective deposition process and the need to tightly control precursor-substrate interactions to enable or prohibit Co deposition on specific areas of the underlying substrate surface, no plasma activation or enhancement of any kind was used. Various cobalt precursors with oxidation states ranging from 1 to 2 were utilized with a substrate temperature in the range of 140–350°C. Co-reactants included H₂, NH₃, (H₂+NH₃) mixture, dimethylhydrazine (DMHz), *t*-butylamine, diethylamine, triethylamine and formic acid, while carrier gases were primarily inert—namely argon (Ar) or nitrogen (N₂). Substrate surface preparation techniques are also critical in area-selective ALD, and included semiconductor [hydrogen-terminated Si, (H-Si)],

insulator [hydroxyl-terminated SiO₂, (OH-SiO₂), low-*k* (*k*~2.6) dielectric carbon-doped oxide (CDO), octadecyltrichlorosilane (OTS)], and metallic surfaces (Cu, Ru, and Pt). Noteworthy investigations and associated findings are discussed below.

Lee et al.⁵⁹ performed a two-phase investigation of the ALD adsorption and reaction mechanisms of bis(N,N'-diisopropylacetamidinato)Co^{II} (Co-206) with either H₂ or NH₃ as co-reactant at a substrate temperature of 350°C. In phase I of the study, Co films were successfully deposited on Si(001) and SiO₂ substrates with either H₂ or NH₃ as co-reactant. However, films grown using NH₃ as co-reactant were metallic and pure Co with little to no N inclusion, while their H₂ counterparts exhibited high oxygen levels. This finding is consistent with the reports on the role of NH₃ radicals in the clean cleavage of Co precursors discussed in Section 7.^{20,51} In phase II of this study, Co films grown by ALD on patterned octadecyltrichlorosilane (OTS) on SiO₂ using either co-reactant formed selectively on SiO₂ but not on OTS, indicating that OTS did effectively block the ALD nucleation and growth process.

Kwon et al.⁶⁰ analyzed the thermal ALD reaction of *t*-butylalylcobalt tricarbonyl (Co-108) with dimethylhydrazine (DMHz) as co-reactant at a substrate temperature of 140°C on OH-terminated SiO₂ and H-terminated Si(111). Unexpectedly, they observed (^tBu-AllylCo(CO)₃) (Co-108) to be substantially more reactive with H-terminated Si than OH-terminated SiO₂. The authors also conducted theoretical calculations that indicated significant differences in the surface reaction energies of Si versus SiO₂—differences which act as the underlying driver for the observed Co source precursor selectivity.

Elko-Hansen et al.⁶¹ examined area-selectivity in ALD Co using bis(N-*t*-butyl-N'-ethylpropionamidinato)Co^(III) (CoAMD) (Co-209) and H₂ as co-reactant at a substrate temperature of 265°C on Cu, SiO₂ and porous low-*k* (*k*~2.6) C-doped oxide (CDO). Adsorption studies showed that Co growth occurred most preferentially on Cu and least preferentially on CDO, and that, similarly to other amidinate precursors, CoAMD (Co-209) readily dissociated on transition metal surfaces such as Cu via a complex dissociative chemisorption mechanism. The investigation also indicated that the CoAMD per-cycle coverage on Cu is ALD-like and self-limited by the slow desorption of amidinate ligands and fragments from the Cu surface. However, significant Cu-Co intermixing by Cu diffusion through grain boundaries in the Co matrix was observed. The Co films also exhibited appreciable C and N contamination. Alternatively, the adsorption of CoAMD on SiO₂ and CDO surfaces seemed to be driven by interactions with exposed OH moieties. Both SiO₂ and CDO favored the formation of oxidized Co²⁺ and possibly Co³⁺ species, as well as some partially reacted CoAMD precursor.

One study by Kerrigan et al.⁶³ carried out a two-phase investigation of area-selective ALD Co from the reaction of bis(1,4-di-*t*-butyl-1,3-diazadienyl)cobalt [Co(^tBuNCHCHN^tBu)₂] (Co-208) with *t*-butylamine, diethylamine or triethylamine as co-reactants at a substrate temperature of 200°C. In phase I, ALD Co growth was observed with *t*-butylamine or diethylamine as co-reactants on conducting (Pt, Ru, and Cu) but not on insulating surfaces (Si(100) with native oxide, thermal SiO₂, H₂ terminated Si and C-doped oxide (CDO)). No growth was achieved with triethylamine as co-reactant on any surface. The authors attributed this behavior to coordination of the amine N atom lone pair to the Co ion to form an adduct consisting of a Co^(II) ion attached to two radical anion diazadienyl ligands. At the deposition temperatures (≥ 160°C), an electron transfer occurred from the two radical anion diazadienyl ligands to the Co^(II) ion, causing the formation of Co metal, *t*-butylamine and two equivalents of 1,4-di-*t*-butyl-1,3-diazadiene (Co-208). They further argued that triethylamine does not contain any N–H bonds, which may be required to provide a similar role to *t*-butylamine and diethylamine. In phase II of this study, the authors performed similar area-selective ALD studies of the reaction of [Co(^tBuNCHCHN^tBu)₂] (Co-208) with *t*-butylamine or diethylamine on patterned substrates consisting of Si(100) substrates with a single, 1000nm-wide by ~60 to 80 nm thick Pt stripe. After 1000 ALD deposition cycles, Co

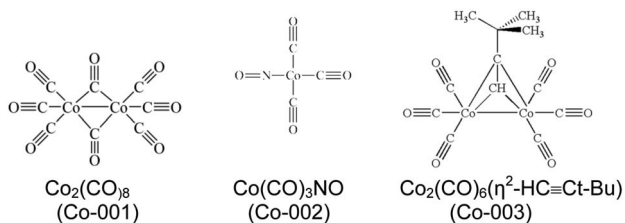
growth was achieved on the Pt stripe but not on the surrounding Si region.

Another study by Kerrigan et al.⁶⁴ examined area-selective ALD behavior in the reaction of bis(1,4-di-*t*-butyl-1,3-diazadienyl)cobalt (Co-208) with formic acid at a substrate temperature of 180°C on Pt, Ru, Cu, Si(100) with native oxide, thermal SiO₂, H₂ terminated Si and CDO. Normal ALD growth was reported on Pt and Cu surfaces even within the first 25 deposition cycles. Alternatively, Co growth was hindered on Ru surfaces for the first 100 cycles, followed by deposition at very low growth rates until 250 cycles, when a higher ALD growth rate was achieved. This behavior indicated a nucleation delay on Ru until surface treatment with formic acid exposed active surface nucleation sites. Once the Ru substrate was covered with an ultrathin Co layer, typical self-limited ALD growth was observed. No Co deposition was observed on Si(100), Si-H and CDO substrates, while films grown on thermal SiO₂ were non-conductive and lacked the metallic texture of Co. Analyses indicated the formation of Co^(II) formate on the SiO₂ surface.

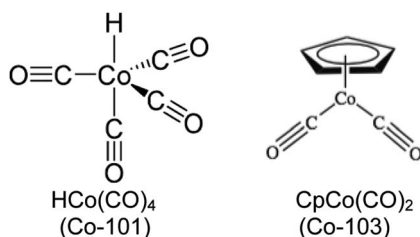
Overview of Cobalt Source Chemistries

The differences in the formation and behavior of cobalt thin films can be attributed in part to fundamental thermodynamic and chemical properties of the source precursors. Table X lists the bond dissociation energies for the indicated bonds in selected cobalt compounds relevant to MOCVD and ALD cobalt. Table XI presents relevant properties of the CVD and ALD cobalt source precursors discussed in this review. The precursors are divided into classes based on the nominal valence (oxidation state) of cobalt. Representative structures of each class are depicted below.

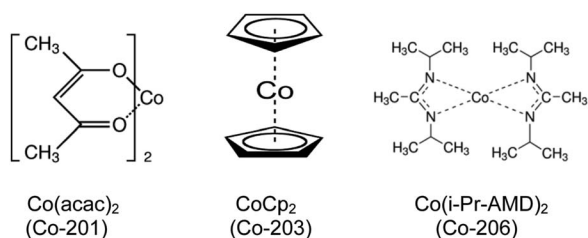
Zero valent cobalt (Co⁰) precursors include cobalt carbonyl compounds such as cobalt carbonyl adducts, dicobalt octacarbonyl, cobalt carbonyl nitrosyl, and cobalt carbonyl *t*-butylacetylene.



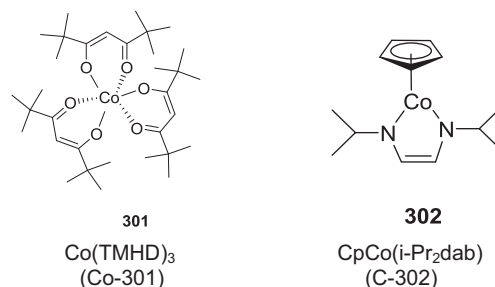
Monovalent cobalt (Co⁺¹) precursors include cobalt carbonyl hydride, and cyclopentadienyl cobalt dicarbonyl.



Divalent cobalt (Co⁺²) precursors include cobalt diketonates, cobaltocenes, and cobalt amidinates.



Trivalent cobalt (Co⁺³) precursors include oxidation state 3, as well as mixtures of oxidation states 2 and 3, such as:



While, in general, the requirement that desirable precursors for CVD and ALD needs to be volatile, stable during storage and transport, and preferably gas or liquid, in the case of cobalt deposition, it should be recognized that many of cobalt precursors are dinuclear (2 cobalt atoms) solids with relatively low volatility. Further, dinuclear complexes are often subject to gas phase nucleation reactions at high vapor pressures and higher temperatures (>200°C).

The performance of cobalt source chemistries for vapor deposition techniques can be most readily anticipated by considering not only the primary cobalt precursor, but the type of co-reactant used, the structure and composition of the substrate surface, and whether the desired film is in a zero oxidation state (cobalt metal or alloys) or a higher oxidation state (cobalt oxides or sulfides).

Co⁰ precursors, the most widely used sources for generating metallic cobalt films, are coordination complexes bearing labile ligands. The success of this class of precursors at depositing pure metallic Co by MOCVD was reported as early as 1999 by Ivanova et al.,³ using the source precursor cobalt tricarbonyl nitrosyl (Co-002). This success can be simplistically associated with the low bond dissociation energies of the ligands (<100kJ/mole) as well as the fact that no formal reduction of the cobalt species is required. Under thermal deposition conditions—namely, non-plasma or radical-induced reactions—precursor behavior during deposition is generally sensitive to carrier gas and substrate surface composition: both the surface interaction of nominally neutral ligands displaced from Co⁰ precursor complexes with the substrate and the mechanisms for the release or elimination of the ligands from the substrate appear to play an important role in film formation.

While deposition of metals is associated with reducing conditions in most cases, mildly oxidative co-reactants are frequently employed that can selectively react with the ligands.

For example, it appears that a carbonyl ligand (CO) can be released from the adsorbed complex by: (i) conversion to carbon dioxide (CO₂) via reaction with oxygen, (ii) conversion to formaldehyde (H₂CO) by reaction with hydrogen, or (iii) conversion to formamide (HCONH₂) by reaction with ammonia. While it is difficult to quantify, cobalt deposition appears to be more sensitive to substrate surface composition and structure than other metal deposition schemes. A recent observation is that some of the Co⁰ precursors such as CCTBA (Co-003) undergo exothermic decomposition at temperature below 200°C while others undergo endothermic decomposition.¹⁰⁵

Deposition on oxides appears to be profoundly different than deposition on metallic substrates, presumably due to differences between the surface electron density of non-metallic and metallic substrates. Copper, for instance, is a far better substrate for metallic cobalt deposition than silicon dioxide. Silicon substrates rich in hydrogen exhibit area specific cobalt deposition, while deposition onto oxidized, hydroxyl containing substrates is suppressed.⁶⁰ Substrates with an affinity for the co-reactants—particularly oxides—can contribute mechanistic pathways for release of the ligands in the deposition of non-metallic cobalt films. It should also be noted that bulk cobalt metal undergoes a transition from hcp to fcc crystalline form at >400°C,⁶⁸ undoubtedly altering the sticking coefficient and adsorption mechanisms of both the precursor and deposition byproducts.

Table XI. Relevant Properties of Recently Studied MOCVD, Pulsed MOCVD and ALD Cobalt Source Precursors

Class (Oxidation state)	Precursor Code	Name	Formula/ Abbreviated Structure	Co wt. %	Molecular Weight	Form*	Melting Point (°C)	Boiling Point (°C/torr)	Vapor Pressure (torr/°C)	CAS#
Co ⁽⁰⁾	Co-001	Dicobalt octacarbonyl ⁸⁵	Co ₂ (CO) ₈	34.47	341.95	S	51° (d)	95°	0.1/45°	10210-68-1
	Co-002	Cobalt tricarbonylnitrosyl ⁸⁵	Co(CO) ₃ NO	34.07	172.97	L	-1.1°	78.6°	91/20°	14096-82-3
	Co-003	Dicobalt hexacarbonyl t-butylacetylene (CCTBA) ⁸⁶	Co ₂ (CO) ₆ (η ² -HC≡Ct-Bu)	32.02	368.07	L		52°/0.8	0.1/40°	56792-69-9
	Co-004	Dicobalt hexacarbonyl trimethylsilylacetylene ^{18,87}	Co ₂ (CO) ₆ (η ² -HC≡CSiMe ₃)	30.68	384.15	S	29°			57032-12-9
	Co-005	Dicobalt hexacarbonyl bis(trimethylsilyl)acetylene ²⁹	Co ₂ (CO) ₆ (η ² -Me ₃ SiC≡CSiMe ₃)	23.75	496.32	S	110° (dec)			14767-82-9
Co ^(I)	Co-101	Hydridocobalt carbonyl ⁸⁵	HCo(CO) ₄	34.27	171.98	L	-33 (d)			16842-03-8
	Co-102	Trifluoromethyl cobalt carbonyl ⁸⁸	CF ₃ Co(CO) ₄	24.56	239.99	L	13°		100/52°	15892-59-8
	Co-103	η ⁵ -Cyclopentadienylcobalt Carbonyl ^{89,90}	CpCo(CO) ₂	32.73	180.05	L	-22°	139-40°	2/38°	12078-25-0
	Co-104	η ⁵ -Pentamethyl cyclopentadienylcobalt dicarbonyl ⁹¹	Cp*Co(CO) ₂	23.55	250.19	S	58°		0.01/40°	12129-77-0
	Co-105	η ⁵ -Cyclopentadienylcobalt bis(ethylene) ⁹²	CpCo(CH ₂ = CH ₂) ₂	32.72	180.13	S				69393-67-5
	Co-106	η ⁵ -Cyclopentadienylcobalt bis(trimethylsilyl)ethylene ⁹³	CpCo[Me ₃ SiCH = CH ₂] ₂	12.57	468.85	S				189282-65-3
	Co-107	η ⁵ -Cyclopentadienyl cobalt 1,5-cyclooctadiene ⁹⁴	Cp(Co(COD))	25.38	232.20	S	103°		~0.1/60°	12184-35-9
	Co-108	(η ³ -t-Butylallyl)cobalt tricarbonyl ⁶⁰	(t-Bu-allyl)Co(CO) ₃	24.54	240.14	L		86°/17		1263431-26-0
	Co-109	Cobalt dicarbonyl[1,3-dihydro-1,3-bis(1-methylene)-2H-imidazol-2-ylidene] nitrosyl ⁴⁰	Co(Dipp ₂ Im)(CO) ₂ (NO)	19.83	297.20	S	44°		0.008/30°	1869928-52-8
	Co-110	Cobalt trimethylphosphinedicarbonyl-[1,3-dihydro-1,3-bis(1-methylene)-2H-imidazol-2-ylidene] nitrosyl ⁴⁴	Co(Dipp ₂ Im)(CO) ₂ (PMe ₃)(NO)	17.06	345.31	S	111°			2205068-13-7
	Co ^(III)	Co-201	Cobalt bis(acetylacetonate) ⁹⁵	Co(acac) ₂	22.91	257.18	S	166-9°		0.01/100°
Co-202		Cobalt bis(2,2,6,6-tetramethylheptan-3,5-dionate)	Co(tmhd) ₂	13.85	425.47	S	143°		0.8/118°	13986-53-3
Co-203		Cobaltocene ^{83,96,97}	CoCp ₂	31.16	189.12	S	173-4°	50°/0.04	0.2/44°	1277-43-6
Co-204		Bis(methylcyclopentadienyl)cobalt	Co(MeCp) ₂	27.14	217.17	S				12146-91-7
Co-205		bis(η ⁵ -pentamethylcyclopentadienyl)-cobalt ^{98,99}	(Cp*) ₂ Co	17.89	329.39	S	>210°			74507-62-3
Co-206		Bis(N,N'-diisopropylacetamidinato) cobalt ¹⁰⁰	Co(i-Pr-AMD) ₂	17.26	341.38	S	84°		0.8/100°	635680-58-9
Co-207		(N,N'-diisopropylacetamidinato)- (η ⁵ -pentamethylcyclopentadienyl) cobalt ¹⁰¹	Cp*Co(i-Pr-AMD)	22.23	265.09	L	7°	65°/0.006		1206524-90-4

Table XI. (Continued).

Class (Oxidation state)	Precursor Code	Name	Formula/ <i>Abbreviated Structure</i>	Co wt. %	Molecular Weight	Form*	Melting Point (°C)	Boiling Point (°C/torr)	Vapor Pressure (torr/°C)	CAS#
	Co-208	Bis(1,4-di-t-butyl-1,3-diazabutadienyl)cobalt ¹⁰²	Co(^t -Bu ² DAD) ₂	14.90	395.47	S	173°		0.05/110°	177099-51-3
	Co-209	N-t-butyl-N-ethylpropinaminato)cobalt ¹⁰³	CoAMD	15.95	369.45	L	-17°		0.55/100°	1011477-51-2
Co(III)	Co-301	Cobalt is tetramethylheptanedionate ¹⁰⁴	Co(tmhd) ₃	9.68	608.75	S	254-6° (dec)		0.5/120°	14877-41-9
	Co-302	η ⁵ -Cyclopentadienyl-N,N'-diisopropyl-1,4-diazabutadienyl cobalt ¹⁷	CpCo(i-Pr ₂ dab)	22.31	264.14	L		100°/0.04		101178-17-0
	Co-303	η ⁵ -Cyclopentadienyl-N,N'-di-t-butyl-1,4-diazabutadienyl cobalt ¹⁷	CpCo(t-Bu ₂ dab)	20.16	292.30	S			0.04/70°	101178-18-1

Data in this table from sources cited or determined by the authors

*L-liquid, S-solid.

A comparison of the generation of metallic cobalt by thermal MOCVD and ALD using Co^0 precursors versus Co^{2+} precursors reveals some general trends: in order to yield metallic Co with Co^{2+} precursors, there seems to be a need for higher substrate temperatures with precisely selected co-reactants, and/or specifically customized substrate surface structure and composition in a narrower process window than when using Co^0 precursors. For example, $\text{Co}(\text{acac})_2$ (Co-201) dissolved in n-propanol solution yielded metallic Co on Ni at substrate temperatures above 250°C, but yielded cobalt carbide when dissolved in isopropanol.⁸ Similarly, $\text{Co}(\text{iPr-MeAMD})_2$ (Co-206) dissolved in tetradecane produced metallic cobalt only with a NH_3/H_2 ratio of 1 at a substrate temperature of 240°C; H_2 alone failed to generate any deposition, while NH_3 alone yielded hcp Co_3N .³² Another general trend is that deposition protocols with added energy sources such as PE-CVD or PE-ALD offer little to no benefit for the deposition of high purity, low resistivity metallic cobalt films due to the fact that other, non-cobalt elemental contaminants are incorporated into the film.

Cobalt precursors in non-zero oxidation states are often preferred for the deposition of non-metallic cobalt films including sulfides, oxides and non-stoichiometric nitrides. While it is appealing to assume that a ligand or adduct bearing an atom of interest could form a binary cobalt compound—e.g., a diketone contributing an oxygen atom to form a cobalt oxide or an amidinate contributing a nitrogen atom to form cobalt nitride—no instances of a single source precursor yielding a targeted film stoichiometry have been reported. As deposition pathways vary widely and the decomposition of the ligands is not straightforward, a co-reactant is required.

This situation is further complicated by the fact that the substrate surface is evolving during the growth process, starting with the initial substrate but transitioning to a cobalt containing surface as a film grows.¹⁰ Yao provides an example of this complexity for amidinates: decomposition of the pyrrolidinate ligand leads to the desorption of several gas-phase products including CH_3CN , HCN and butene from the metals, as well as CO and CO_2 from the oxygen-containing surfaces; in all cases, dehydrogenation of the organic moieties is accompanied by hydrogen removal, mainly in the form of H_2 from metallic surfaces and as water from metal oxide surfaces; however, the threshold for this reaction varies wildly: from 270 K on Ni(110) to 430 K on O/Cu(110), 470 K on Cu(110), 500 K on NiO/Ni(110) and 570 K on SiO_2/Ta .

Cyclopentadienyl ligands (Cp) almost always are problematic. While this class of compounds has excellent storage and transport properties, the high energy barriers for homolytic bond dissociation for cobaltocenes (dicyclopentadienylcobalt compounds; CpCo-Cp (Co-203): 341.6 kJ/mol) almost always exhibit alternate decomposition pathways that result in the incorporation of carbon.⁵¹

The performance of Co^0 compounds remains the most advantageous for thermally-induced metallization schemes. However, the advantage of Co^0 compounds is mitigated the introduction of plasma causes precursor decomposition by ionization prior to neutral compound bond dissociation. In higher valent cobalt binary thin films such as cobalt oxides and sulfides, ionizing methods are more likely to generate acceptable film qualities. Alternatively, Co^0 precursors are less likely to produce optimum properties for binary films due to gas phase depletion reactions initiated in the ionizing environments.

Summary and Commentary

This article has reviewed the most recent published work on MOCVD, plasma and thermal ALD, and pulsed MOCVD Co technologies, with an emphasis on important new advances in Co thin film systems focused on Co source precursors, mechanistic and modeling studies, transport and delivery techniques, thin film growth processes, and their resulting effects on film properties. Innovative approaches to Co deposition were also discussed, including electrochemical ALD (e-ALD), area-selective ALD and two-step processes for the formation of metallic Co. The volume of work examined indicates that Co is the target of an expanding body of research and development

(R&D) efforts, especially as it enters main stream IC manufacturing technologies.

While generalizations are difficult when such a wide range of Co oxidation states, chemistries and applications are considered, some common trends can be identified from a chemistry perspective. Although exceptions exist, the most general, fully anticipated trend is that metallic cobalt films are more readily deposited using lower oxidation state cobalt precursors— Co^0 in particular—and that higher oxidation state cobalt precursors are generally more amenable to the formation of binary cobalt compound films. Departures from this simple paradigm are generally associated with strategies that involve substrate interaction, film thickness and conformality requirements.

From a processing perspective, the evolution in Co deposition methodology generally mirrors that of many other material systems as the technological drive continues toward sub-nanometer scale devices and structures. The latter require exact atomic level control of the composition, uniformity and morphology of exceedingly thin Co layers, down to a thickness of a few atoms. As a result, Co deposition techniques have gradually migrated from traditional MOCVD to ALD processes in light of the need for exceedingly thin cobalt films which must be deposited uniformly, continuously and coherently.⁶⁹ As a rather simplistic example of this need, a 2nm-thick Co film will consist of a layer only ~ 15 atoms thick; while MOCVD produces inherently poor step coverage due to device structures becoming substantially more complex, with higher aspect ratio and narrower channels, vias and trenches, ALD has the intrinsic capacity to offer precise atomic level control and exceptional conformality for cobalt ultrathin films in nanoscale IC device structures.

Finally, two additional trends in Co deposition techniques are also worth noting. The first is area-specific or area-selective Co thermal ALD, which is characterized by the ability to catalyze or prevent Co deposition on specific areas of the substrate: specifically-designed Co source precursors are made to interact preferentially with pre-treated substrate surface patterns and geometries to yield Co films only on the targeted regions of the substrate surface. The second is pulsed MOCVD, wherein the co-reactants get pulsed simultaneously into the reaction zone, thus providing the potential to combine the advantages of both MOCVD and ALD. Both trends are still in their infancy, and significant future R&D efforts will be required to assess their manufacturability. Concurrently, the field of Co deposition methods is expected to benefit from the introduction of new atomic and molecular level surface treatment and film deposition protocols such as Molecular Layer deposition (MLD) and self-assembled monolayers (SAMs).

ORCID

Barry Arkles  <https://orcid.org/0000-0003-4580-2579>

References

1. A. Kafizas, C. J. Carmalt, and I. P. Parkin, *Coord. Chem. Rev.*, **257**, 2073 (2013).
2. Y. Nakamura, in *ECS Transactions*, **3**, 29, ECS (2007).
3. A. R. Ivanova et al., *J. Electrochem. Soc.*, **146**, 2139 (1999).
4. A. E. Kaloyeros, A. Londergan, and B. Arkles, *US Pat.* 6,346,477 (2002).
5. F. Zaera, *Coord. Chem. Rev.*, **257**, 3177 (2013).
6. D. J. H. Emslie, P. Chadha, and J. S. Price, *Coord. Chem. Rev.*, **257**, 3282 (2013).
7. S. D. Elliott, G. Dey, and Y. Maimaiti, *J. Chem. Phys.*, **146**, 052822 (2017).
8. P. A. Premkumar, A. Turchanin, and N. Bahlawane, *Chem. Mater.*, **19**, 6206 (2007).
9. N. D. Papadopoulos, E. Illekova, H. S. Karayanni, and E. Hristoforou, *J. Optoelectron. Adv. Mater.*, **10**, 1098 (2008).
10. K. Lee et al., *Jpn. J. Appl. Phys.*, **47**, 5396 (2008).
11. D. Lammers, *Semicond. Manuf. Des. Community*, (2017) semimd.com/blog/2017/12/21.
12. P. Singer, *Semicond. Des. Manuf. Community*, (2018) <http://semimd.com/blog/tag/cobalt/>.
13. A. R. Londergan et al., *J. Electrochem. Soc.*, **148**, C21 (2001).
14. S. I. Dorovskikh et al., *Surf. Eng.*, **32**, 8 (2016).
15. N. Samal, K. B. Chetry, K. Rook, A. Hayes, and A. Devasahayam, *J. Vac. Sci. Technol. B. Nanotechnol. Microelectron. Mater. Process. Meas. Phenom.*, **32**, 011206 1–5 (2014).

16. J. A. Hamilton, T. Pugh, A. L. Johnson, A. J. Kingsley, and S. P. Richards, *Inorg. Chem.*, **55**, 7141 (2016).
17. T. Pugh, S. D. Cosham, J. A. Hamilton, A. J. Kingsley, and A. L. Johnson, *Inorg. Chem.*, **52**, 13719 (2013).
18. C. Georgi, A. Hildebrandt, A. Tuchscherer, S. Oswald, and H. Lang, *Zeitschrift für Anorg. und Allg. Chemie*, **639**, 2532 (2013).
19. C. Georgi et al., *Thin Solid Films*, **578**, 180 (2015).
20. B. K. Ramos, M. J. Saly, and Y. J. Chabal, *Coord. Chem. Rev.*, **257**, 3271 (2013).
21. A. C. Frank and P. T. A. Sumodjo, *Electrochim. Acta*, **132**, 75 (2014).
22. C. Q. Cui, S. P. Jiang, and A. C. C. Tseung, *J. Electrochem. Soc.*, (1990).
23. K. Nakaoka, M. Nakayama, and K. Ogura, *J. Electrochem. Soc.*, (2002).
24. Q. Huang, T. W. Lyons, and W. D. Sides, *J. Electrochem. Soc.*, (2016).
25. M. R. Khelladi, L. Mentar, M. Boubatra, A. Azizi, and A. Kahoul, *Mater. Chem. Phys.*, **122**, 449 (2010).
26. K. Venkatraman, Y. Dordi, and R. Akolkar, *J. Electrochem. Soc.*, **164**, D104 (2017).
27. E. A. Owen and D. M. Jones, *Proc. Phys. Soc. Sect. B*, **67**, 456 (1954).
28. D. H. Buckley and L. Johnson Robert, *NASA Tech. Note*, **TN D-2523** (1964).
29. C. Georgi et al., *J. Mater. Chem. C*, **2**, 4676 (2014).
30. K. Shima, H. Shimizu, T. Monose, and Y. Shimogaki, *ECS J. Solid State Lett.*, **3**, P20 (2014).
31. T. Weiss, V. Zielasek, and M. Bäumer, *Sci. Rep.*, **5**, 18194 (2015).
32. J. Yang, K. Li, J. Feng, and R. G. Gordon, *J. Mater. Chem. C*, **3**, 12098 (2015).
33. Y. Zhang, L. Du, X. Liu, and Y. Ding, *New J. Chem.*, **42**, 9110 (2018).
34. H. Shimizu, K. Sakoda, and Y. Shimogaki, *Microelectron. Eng.*, **106**, 91 (2013).
35. M. C. Karunaratne, T. J. Knisley, G. S. Tunstall, M. J. Heeg, and C. H. Winter, *Polyhedron*, **52**, 820 (2013).
36. J. Park et al., *J. Energy Chem.*, **22**, 403 (2013).
37. J. H. Park et al., *Surf. Coatings Technol.*, **259**, 98 (2014).
38. T. D. M. Elko-Hansen, A. Dolocan, and J. G. Ekerdt, *J. Phys. Chem. Lett.*, **5**, 1091 (2014).
39. J. P. Klesko, M. M. Kerrigan, and C. H. Winter, *Chem. Mater.*, **28**, 700 (2016).
40. F. Hering et al., *Organometallics*, **35**, 2806 (2016).
41. J. You and Y. Guo, *J. Alloys Compd.*, **758**, 116 (2018).
42. K. Väyrynen et al., *Chem. Mater.*, **30**, 3499 (2018).
43. T. Nam et al., *J. Alloys Compd.*, **737**, 684 (2018).
44. K. Lubitz et al., *Organometallics*, **37**, 1181 (2018).
45. K. B. Klepper, O. Nilsen, and H. Fjellvåg, *Thin Solid Films*, (2007).
46. M. F. J. Vos, G. van Straaten, W. M. M. E. Kessels, and A. J. M. Mackus, *J. Phys. Chem. C*, **122**, 22519 (2018).
47. S. T. Barry, A. V. Teplyakov, and F. Zaera, *Acc. Chem. Res.*, **51**, 800 (2018).
48. M. Diskus, O. Nilsen, and H. Fjellvåg, *Chem. Vap. Depos.*, **17**, 135 (2011).
49. E. Rauwel et al., *Chem. Vap. Depos.*, **18**, 315 (2012).
50. B. Han, K. H. Choi, K. Park, W. S. Han, and W.-J. Lee, *Electrochem. Solid-State Lett.*, **15**, D14 (2011).
51. J. Yoon et al., *J. Electrochem. Soc.*, **158**, H1179 (2011).
52. L. C. Kalutarage, P. D. Martin, M. J. Heeg, and C. H. Winter, *J. Am. Chem. Soc.*, **135**, 12588 (2013).
53. L. C. Kalutarage, P. D. Martin, M. J. Heeg, and C. H. Winter, *Inorg. Chem.*, **52**, 5385 (2013).
54. T. J. Knisley, L. C. Kalutarage, and C. H. Winter, *Coord. Chem. Rev.*, **257**, 3222 (2013).
55. J. M. Kim et al., *Jpn. J. Appl. Phys.*, **49**, 5S2 (2010).
56. B. S. Lim, A. Rahtu, and R. G. Gordon, *Nat. Mater.*, (2003).
57. H.-B.-R. Lee and H. Kim, *ECS Trans.*, **16**, 219 (2008).
58. K. Kim et al., *Jpn. J. Appl. Phys.*, **46**, L173 (2007).
59. H.-B.-R. Lee et al., *J. Electrochem. Soc.*, **157**, D10 (2010).
60. J. Kwon, M. Saly, M. D. Halls, R. K. Kanjolia, and Y. J. Chabal, *Chem. Mater.*, **24**, 1025 (2012).
61. T. D. Elko-hansen, *Chem. Mater.*, **26**, 2642 (2014).
62. S. D. Elliott et al., *Adv. Mater.*, **28**, 5367 (2016).
63. M. M. Kerrigan, J. P. Klesko, and C. H. Winter, *Chem. Mater.*, **29**, 7458 (2017).
64. M. M. Kerrigan et al., *J. Chem. Phys.*, **146**, 052813 (2017).
65. H.-B.-R. Lee and H. Kim, *Electrochem. Solid-State Lett.*, **9**, G323 (2006).
66. K. Hyungjun et al., *J. Korean Phys. Soc.* (2010).
67. S. Pasko, L. G. Hubert-Pfalzgraf, A. Abrutis, and J. Vaissermann, *Polyhedron*, **23**, 735 (2004).
68. F. G. Hodge, *Kirk-Othmer Encycl. Chem. Technol.*, Editor M. H. Kroschwitz, **6**, 760 (1993).
69. E. Ahvenniemi et al., *J. Vac. Sci. Technol. A*, **35**, 10801 (2017).
70. G. Govindasamy, P. Murugasen, and S. Sagadevan, *Mater. Res.*, **20**, 60 (2017).
71. A. S. Andreev, J. B. D'Espinoza De Lacaille, O. B. Lapina, and A. Gerashenko, *Phys. Chem. Chem. Phys.*, **17**, 14598 (2015).
72. N. Kumar, N. Raman, and A. Sundaresan, *Zeitschrift für Anorg. und Allg. Chemie* (2014).
73. K. V. Rao and A. Smakula, *J. Appl. Phys.* (1965).
74. L. D. Kadam and P. S. Patil, *Thickness-dependent properties of sprayed cobalt oxide thin films*, p. 225, (2001).
75. S. Schmid, R. Hausbrand, and W. Jaegermann, *Thin Solid Films*, **567**, 8 (2014).
76. J. Dean, *Lange's Handbook of Chemistry*, 15th ed., McGraw-Hill Inc., (1999).
77. R. Walsh, in *Silicon Compounds: Silanes and Silicones*, B. C. Arkles and G. L. Larson, Editors, p. 200, Gelest (2008).
78. C.-C. Ye, L.-F. Xie, and X.-H. Ju, *Phosphorus. Sulfur. Silicon Relat. Elem.*, **186**, 1948 (2011).
79. Y. R. Luo, *Comprehensive Handbook of Chemical Bond Energies*, 1st ed., CRC Press, (2007).
80. X. Gong, Q. S. Li, Y. Xie, R. B. King, and H. F. Schaefer, *New J. Chem.* (2009).
81. B. Sztáray, L. Szepez, and T. Baer, *J. Phys. Chem. A* (2003).
82. D. B. Jacobson and B. S. Freiser, *J. Am. Chem. Soc.*, **107**, 7399 (1985).
83. J. Opitz, *Electron impact ionization of cobalt-tricarbonyl-nitrosyl, cyclopentadienyl-cobalt-dicarbonyl and biscyclopentadienyl-cobalt: appearance energies, bond energies and enthalpies of formation*, p. 115, (2003).
84. C. A. Cooper, S. Ivanov, and M.-S. Kim, (2018).
85. P. Gilmont, A. A. Blanchard, C. M. Mason, and R. L. Barnard, in *Inorganic Syntheses*, (2007).
86. P. Galow, A. Sebald, and B. Wrackmeyer, *J. Organomet. Chem.* (1983).
87. N. E. Schore, *Organic Reactions*, Wiley, Hoboken, (1991).
88. W. Hieber, W. Beck, and E. Linder, *Zeitschrift für Naturforsch.*, **16b**, 229 (1961).
89. E. O. Fischer and H. Leipfinger, *Zeitschrift für Naturforsch.*, **10b**, 353 (1955).
90. T. S. Piper, F. A. Cotton, and G. Wilkinson, *J. Inorg. Nucl. Chem.* (1955).
91. S. A. Frith, J. L. Spencer, W. E. Geiger Jr., and J. Edwin, *Inorg. Synth.* (1985).
92. K. Jonas, *Angewandte Chemie Suppl.*, 1005 (1983).
93. M. Hapke, N. Weding, and A. Spannenberg, *Organometallics*, **29**, 4298 (2010).
94. R. B. King, P. M. Treichel, and F. G. A. Stone, *J. Am. Chem. Soc.*, **83**, 3593 (1961).
95. J. B. Ellern, R. O. Ragsdale, R. J. Allen, A. B. Chatterjee, and D. F. Martin, *Inorg. Synth.* (1968).
96. E. O. Fischer and R. Jira, *Zeitschrift für Naturforsch.*, **8b**, 327 (1953).
97. L. A. Torres-Gómez, G. Barreiro-Rodríguez, and F. Méndez-Ruiz, *Thermochim. Acta* (1988).
98. U. Kölle and F. Khouzami, *Angew. Chemie*, **92**, 658 (1980).
99. J. L. Robbins, N. Edelstein, B. Spencer, and J. C. Smart, *J. Am. Chem. Soc.*, **104**, 1882 (1982).
100. B. S. Lim, A. Rahtu, J.-S. Park, and R. G. Gordon, *Inorg. Chem.*, **42**, 7951 (2003).
101. C. Lansalot-Matras, C. Dussarat, V. Omarjee, and C. Hsiao, *U. S. Pat.* 8,349,738 (2013).
102. T. J. Knisley, M. J. Saly, M. J. Heeg, J. L. Roberts, and C. H. Winter, *Organometallics*, **30**, 5010 (2011).
103. D. V. Shenai, M. Bierman, R. DiCarlo, and G. Doherty, and , in *ALD Conference 2014*, Kyoto (2014).
104. M. A. Siddiqi, R. A. Siddiqi, and B. Atakan, *Surf. Coatings Technol.* (2007).
105. A. Cooper, V. Ivanov, and M. Kim, *U. S. Pat. Appl.* 2018/0B74738, (2018).